

**Evaluation of the Optical Autocovariance Wind Lidar (OAWL) and its
Potential Impact on Numerical Weather Prediction**

Final Report

Principal investigator: Dr. Robert Atlas, Director
NOAA Atlantic Oceanographic and Meteorological Laboratory
4301 Rickenbacker Causeway
Miami, FL 33149-434-979-3571
robert.atlas@noaa.gov; ph: 305-361-4300

Co-Investigators: Dr. G. D. Emmitt
Simpson Weather Associates,
809 East Jefferson Street
Charlottesville, VA 22902

Dr. Michael Hardesty
NOAA ESRL Chemical Sciences Division
Boulder, CO 80309

Mr. Eric Kemp
Science Systems and Applications Inc
NASA Goddard Space Flight Center
Greenbelt, MD 20771

Dr. Lars Peter Riishojgaard
Joint Center for Satellite Data Assimilation
5200 Auth Rd, room 808
Camp springs MD 20746

Dr. Tom Clune
NASA Goddard Space Flight Center
Greenbelt, MD 20771

Dr. Sara Tucker
Ball Aerospace & Technologies Corp.
Boulder, CO 80301

Period of Performance: June 1, 2012 – September 30, 2013

1. Introduction

The primary objectives of this project were to evaluate the relative advantages and potential impact of two alternative wind lidar technologies and also to determine if the previously developed Sensor Web OSSE system could be used to answer key questions related to observing system design and utility. The research that we proposed consisted of the following major activities:

1. Construct a conceptual model for a space-based Optical Autocovariance Wind Lidar OAWL/FI. Three levels of confidence were planned: space-based system performance scaled from demonstrated performance with ground and/or airborne system; performance scaled with use of SOTA hardware and proven performance; and, performance using projected improvements in key hardware components (optics, detectors, etc).
2. Generate a realistic data product (~ 2 weeks of simulation) for a space-based OAWL/FI using the ECMWF's T511 Nature Run (NR) with the Doppler Lidar Simulation Model (DLSM) currently operating through the GSFC Software Systems Support Office (SSSO) portal. Produce a similar data set for the GSFC's fvGCM NR.
3. Compare the OAWL/FI data products with those generated for a hybrid DWL using the same NRs and DLSM. These comparisons were to be aimed at providing a very good first order sense of the advantages and disadvantages of the OAWL/FI relative to the current "hybrid DWL" concept that had gone through NASA/GSFC's IDL/MDL, and had subsequently been assessed through global OSSEs done by the Joint Center for Satellite Data Assimilation (JCSDA) under NASA funding provided under the Wind Lidar Science element of ROSES 2007.
4. Conduct an initial impact study using the DLSM to generate an extended set of simulated OAWL/FI data for a one- three month period using the fvGCM NR. These impact studies were to be conducted at the SSSO.
5. If warranted, conduct a full global OSSE to assess the relative impact of OAWL/FI and the original concept for a hybrid DWL on global atmospheric analyses and numerical weather prediction, which would utilize the ECMWF T511 NR and the OSSE system, and the GDAS used by the JCSDA for their OSSE work.
6. If warranted, conduct a regional OSSE to assess the relative impact of OAWL/FI and 3DWINDS on hurricane track and intensity prediction using the 1km resolution WRF ARW NR embedded within the ECMWF T511, and NOAA's operational hurricane forecast model (HWRF).

In this report, we summarize the work that was completed with regard to each of these tasks. Section 2 reviews OSSE methodology and earlier experiments conducted at NASA GSFC. Section 3 presents the 3 OSSE systems used in this study. Section 4 describes the lidar systems and the unique and very realistic simulation of lidar data that we performed. Section 5 presents a pre-OSSE evaluation of the different lidars that we studied in this investigation. Sections 6, 7, and 8 present the main results of the global and regional OSSEs that we conducted. A summary of the project with recommendations is given in section 9. Finally, reports prepared by Ball Aerospace as a part of this project are included separately as an appendix to this report.

The following scientists supported the principal investigator and co-investigators in the performance of this project and made very significant contributions to this study: Tomislava Vukicevic, Lisa Bucci, Bachir Annani, Altug Aksoy, Javier Delgado, Sundara Gopalakrishnan, and Xuejin Zhang at NOAA AOML; Sid Wood and Steve Greco at SWA; Zhaizhong Ma and Michiko Masutani at JCSDA, Bob Rosenberg, Juan-Carlos Jusem and Josse Jacob at NASA GSFC.

2. The OSSE concept

Observing System Simulation Experiments (OSSEs) are an important tool for evaluating the potential impact of proposed new observing systems, as well as for evaluating trade-offs in observing system design, and in developing and assessing improved methodology for assimilating new observations. Extensive OSSEs have been conducted at NASA/ GSFC (and more recently at NOAA/AOML) in collaboration with Simpson Weather Associates and operational data assimilation centers from 1985-2005. As described below, these OSSEs determined correctly the quantitative potential for several proposed satellite observing systems to improve weather analysis and prediction prior to their launch, evaluated trade-offs in orbits, coverage and accuracy for space-based wind lidars, and were used in the development of the methodology that led to the first beneficial impacts of satellite surface winds on numerical weather prediction. These earlier OSSEs contributed substantially to the extension of useful forecast skill, from 2-3 days initially to 5-10 days at the present time.

Although there are many possibilities for how an Observing System Experiment (OSE) may be conducted, the most typical procedure is as follows: First a "Control" data assimilation cycle is performed. This is followed by one or more experimental assimilations in which a particular type of data (or specific observations) are either withheld or added to the Control. Forecasts are then generated from both the Control and experimental assimilations every few days (to achieve relative independence of the forecast sample). The analyses and forecasts from each assimilation are then verified and compared in order to determine the impact of each data type being evaluated. Experiments performed in this manner provide a quantitative assessment of the value of a selected type of data to the specific data assimilation system (DAS) that was used. In addition, the OSE also provides useful information on the effectiveness of the DAS. This information can be used to improve the utilization of this and other data in the DAS, as well as to determine the value of the data.

The methodology currently used for OSSEs is very similar to that described above for OSEs and was refined in the early 1980's by the principal investigator to increase the realism and usefulness of such experiments (Atlas et al., 1985a,b; Atlas, 1997). In essence, an OSSE system consists of the following elements (shown schematically in Figure 1):

(1) A long atmospheric model integration using a very high resolution "state of the art" numerical model to provide a complete record of the assumed "true" state of the atmosphere referred to as the "nature run" or "reference atmosphere". For the OSSE to be meaningful, it is essential that the nature run be realistic, i.e. possess a model climatology, average storm tracks, etc. that agrees with observations to within pre-specified limits.

(2) Simulated conventional and space-based observations from the nature run. All of the observations should be simulated with observed (or expected) coverage, resolution, and accuracy. In addition, bias and horizontal and vertical correlations of errors with each other and with the synoptic situation should be introduced appropriately. Two approaches have been used for this purpose. The simpler approach is to interpolate the nature run values to the observation locations and then add appropriate errors. The more complicated (and expensive) approach is to attempt to retrieve observations from the nature run in the same way as observations are retrieved in the real atmosphere.

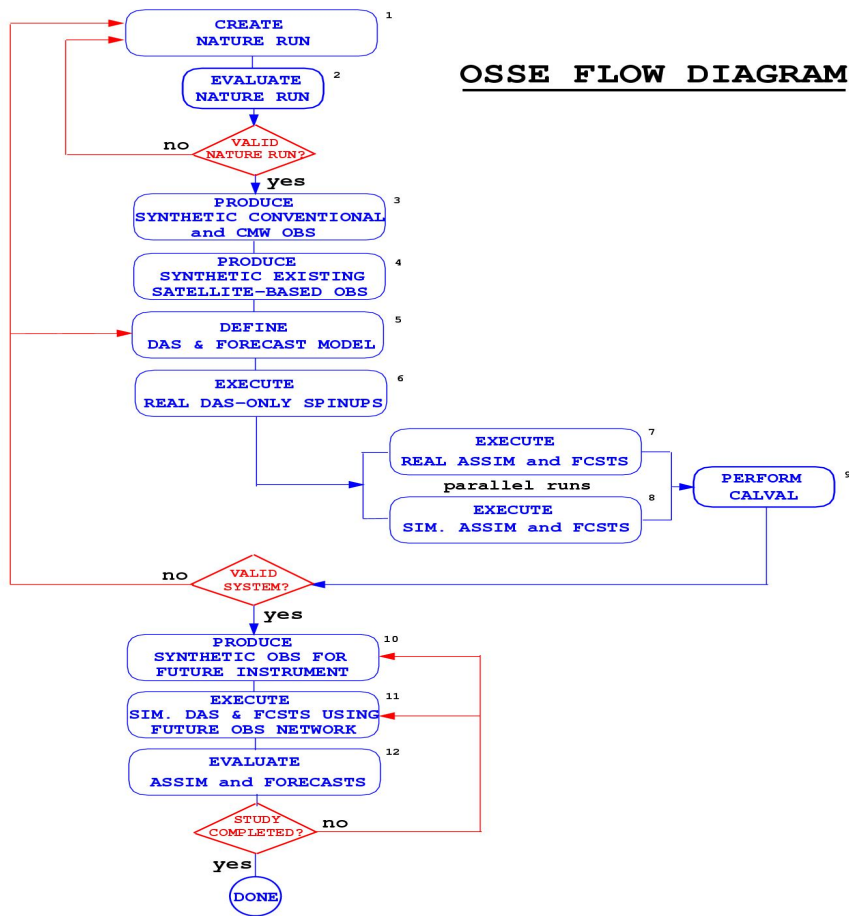


Figure 1. Schematic of the OSSE elements and process.

(3) Control and experimental data assimilation cycles. These are identical to the assimilation cycles in an OSE except that only simulated data are assimilated. In order to avoid the identical twin problem, a different model from that used to generate the nature run is used for assimilation and forecasting. Typically this model has less accuracy and resolution than the nature model. Ideally, the differences between the assimilation and nature models should approximate the differences between a "state of the art" model and the real atmosphere.

(4) Forecasts produced from the Control and Experimental assimilations.

As with the OSE's, forecasts are generated every few days to develop an independent sample. The analyses and forecasts are then verified against the nature run to obtain a quantitative estimate of the impact of proposed observing systems and the expected accuracies of the analysis and forecast products that incorporate the new data.

An important component of the OSSE that improves the interpretation of results is validation against a corresponding OSE. In this regard, the accuracy of analyses and forecasts and the impact of already existing observing systems in simulation is compared with the corresponding accuracies and data impacts in the real world. Ideally, both the simulated and real results should be similar. Under these conditions, no calibration is necessary and the OSSE results may be interpreted directly. If this is not the case, then calibration of the OSSE results can be attempted by determining the constant of proportionality between the OSE and OSSE impact.

An extensive series of OSSEs was conducted from 1985 to 2005 using the above methodology. These OSSEs evaluated quantitatively:

(1) the relative impact of temperature, wind and moisture profiles from polar orbiting satellites (These experiments showed wind data to be more effective than mass data in correcting analysis errors and indicated significant potential for space-based wind profile data to improve weather prediction.)

(2) the relative importance of upper and lower level wind data (These experiments showed that the wind profile data from 500hpa and higher provided most of the impact on numerical forecasting with the Goddard Laboratory for Atmospheres global model.)

(3) different orbital configurations and the effect of reduced power for the space-based laser wind sounder (These experiments showed the quantitative reduction in impact that would result from proposed degradation of the LAWS instrument.)

(4) the relative impact of the ERS and NSCAT scatterometers prior to their launch (This relative impact was confirmed after the launch of these instruments.)

(5) the quantitative impact of AIRS and the importance of cloud clearing (This was also confirmed with real AIRS data after the launch of the Aqua satellite.)

In addition, OSSEs were used to:

(1) develop and test improved methodology for assimilating both passive and active microwave satellite surface wind data (This led to the first beneficial impact of scatterometer data on numerical weather prediction, as well as to the assimilation of SSM/I wind speed data.)

(2) determine the specific requirements for space-based lidar winds for the Global Tropospheric Wind Sounder (GTWS) mission.

3. The OSSE systems used in this study

a. GEOS 5 DAS/fvGCM Nature run

SSSO has maintained a rudimentary OSSE system as part of the Sensor Web Simulator (SWS) software package (Talabac et al 2011). The Goddard Earth Observing System Data Assimilation System (GEOS-DAS; Rienecker et al 2008) is a global data assimilation and forecasting system that combines the NASA GEOS-5 atmospheric general circulation model with the NOAA/NASA Gridpoint Statistical Interpolation (GSI) program. GEOS-5 is configured to run at 0.5-degree by 0.667-degree resolution with a model top of 0.01 mb. The GSI performs a multivariate 3-D variational analysis (3DVAR) at the same resolution using short-term GEOS-5 forecasts as the background. Observations obtained within a +/- 3 hour time window centered on the nominal analysis time (00, 06, 12, or 18 UTC) are assimilated, with off-time observations matched with temporally interpolated background fields. GSI analyses are then used to adjust GEOS-5 via the Incremental Analysis Update (IAU) technique (Bloom et al 1996). Here GEOS-5 is initialized from an earlier restart file, and the analysis increments are used to specify extra tendencies terms in the prognostic equations. GEOS-5 will run for 6 hours with these tendencies (termed the “corrector mode”). At the end of the corrector mode, a new restart file is written and the model runs another 6 hours to produce a new background, as shown in figure 2. In our experiments, GEOS-5 is then run at 00 UTC without IAU for a 5-day period to produce synthetic forecasts.

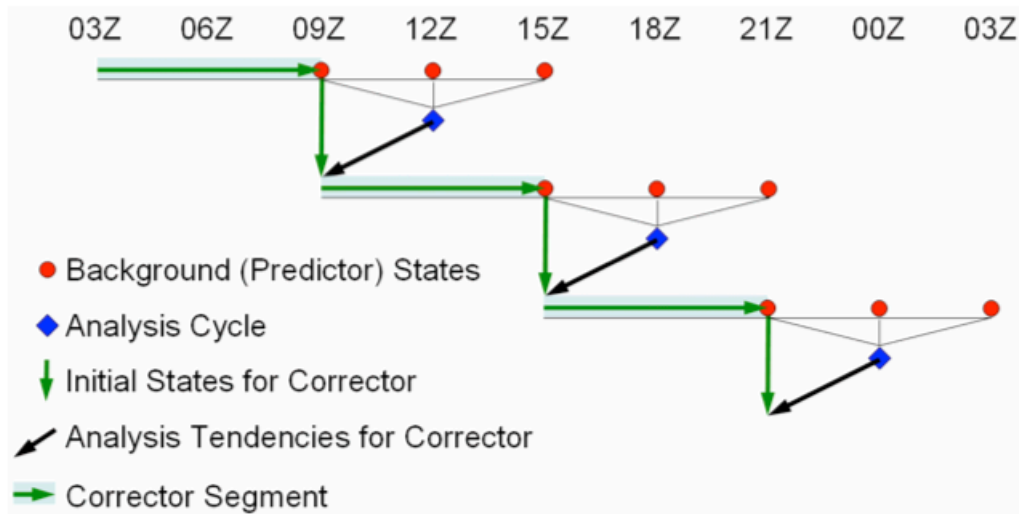


Figure 2: The forecast-analysis cycle used with GEOS-DAS. From Rienecker et al (2008).

The fvGCM Nature Run is a 0.5-degree resolution continuous simulation with three-hourly output over a period of three and a half months. It has been used in prior lidar OSSE work with the GEOS-3 data assimilation system for which an extensive validation had been performed (Atlas and Riishojgaard, 2008; Atlas and Emmitt, 2008; Atlas, 2012; Atlas et al, 2013). Synthetic observations derived from the fvGCM Nature Run include surface observations, rawinsondes, satellite-derived temperature retrievals, aircraft reports, cloud drift winds

(SATWIND) and ASCAT scatterometer data. For this study, the SATWIND and ASCAT data were replaced with synthetic GOES-R cloud drift winds and “perfect QuikSCAT” scatterometer data generated during the Sensor Web project (Talabac et al 2011). It was felt that these newer data types would more accurately represent the collection of observing systems that would exist when a space-based DWL might be deployed.

It should be noted that the GEOS-5 DAS/fvGCM OSSE system has significant drawbacks. First, unlike the GEOS-3/fvGCM OSSE system, the GEOS-5 OSSE system was never validated. Second, the top of the GEOS-5 model is 0.01 mb, significantly higher than the 4.5-mb top of the fvGCM nature run. Third, there are no satellite radiances available for assimilation in this data set. Finally, the version of GSI included in GEOS-DAS does not have a functioning line-of-sight (LOS) operator, thus requiring assimilation of 2-D horizontal wind vectors *derived from* collocated LOS measurements.

The SWS was designed to use the GEOS-5 DAS/fvGCM for “Sensor Web” OSSEs, i.e., studies with dynamically adjusting and interacting observing systems where viewing angles and observation collection might vary (Talabac et al 2011). Thus the full SWS includes interfaces to automate calculation orbit positions, viewing angles, and shot positions (via AGI’s Satellite Tool Kit; see <https://www.agi.com>); calculation of synthetic observations via SWA’s DLMS and related models; and conversion to BUFR format (World Meteorological Organization 2011) used by the GSI. For this project, such advanced features were unnecessary and so were disabled. A feature that was preserved, however, was the use of a GUI to set experiment options (e.g., selection of lidar data for assimilation), submit experiments, and monitor experiment progress.

b. NCEP GFS/ECMWF T511 Nature run

The OSSE system currently utilized by the Joint Center for Satellite Data Assimilation (JCSDA) utilizes the FY 12 version of the National Center for Environmental Prediction (NCEP) Gridpoint Statistical Interpolation/Global Forecast System (GSI/GFS), and an ECMWF T511 nature run. The experiment setting is consistent with the operational GSI/GFS system at NCEP but a model resolution of T382L64 (i.e., spectral triangular truncation 382 with 64 layers) has been used. A short term forecast (6 hours) is run to obtain a first guess for the data assimilation, which uses a larger ± 3 hour data cutoff window, and the analyses and forecasts are centered at 0000, 0600, 1200 and 1800 UTC.

The lidar wind operator has been developed and tested to assimilate the LOS lidar measurements within the GSI data assimilation system. The observation operator for horizontal line-of-sight winds is relatively simple, consisting of an interpolation of the horizontal wind component of the background field to the observation time and location, followed by a projection on the line of sight of the lidar. The analysis is obtained by minimizing the scalar cost function:

$$J(x) = \frac{1}{2}(x - x_b)^T B^{-1}(x - x_b) + \frac{1}{2}(y - H[x])^T R^{-1}(y - H[x]) \quad (1)$$

where the vector x_b represents the background or prior estimate of the control vector x , and $x = x_a$ (analysis state) when minimized; B is the background error covariance matrix; R is

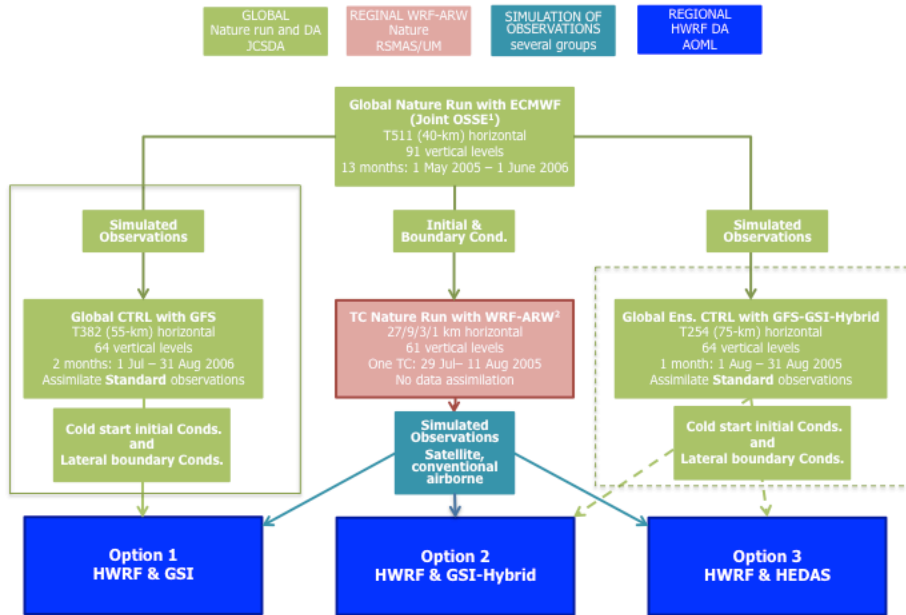
the observational and representativeness error covariance matrix; the vector \mathbf{y} contains the available observations, e.g., lidar wind data in this OSSE; and $H[x]$ is the observations operator that transforms from the model state to the observation space as described above.

c. HWRF-HDAS/T511-ARW Nature run

The regional OSSE system (for Tropical Cyclone OSSEs) was initiated under the Sensor Web Project and has been further developed at AOML under this proposal, using the HWRF model (Hurricane Weather Research and Forecasting model). The regional OSSE system includes the following 4 major components:

1. HWRF forecast system that is equivalent to NOAA's operational hurricane prediction system. In the OSSEs, the HWRF model is configured with 2 grids: the outer-parent and storm-following-inner grids, with spatial resolution of, respectively, 9 and 3 km. This grid configuration is more advanced than for the operational forecast system, which currently uses 27 km resolution for the outer domain. The lateral boundary conditions for the regional domain are obtained from the GFS (Global Forecast System) simulations performed at the JCSDA.
2. Data Assimilation system: The HWRF-OSSE system includes three data assimilation options. These are: (a) GSI (Gridpoint Statistical Interpolation), (b) Hybrid EnKF-GSI and (c) HWRF Ensemble Data Assimilation (HEDAS). In the initial experiments reported here, only the first option (GSI) is used.
3. Simulated observation data source: This can be based on either the global or regional nature simulations.
4. Regional nature data for verification: The regional nature for these experiments was generated by embedding the WRF ARW model at 1 km resolution within the ECMWF T511 global nature. It covers a 13-day period that includes tropical cyclone formation and the rapid intensification of a major hurricane. A detailed description of the realism of this nature run is given by Nolan et al. (2013) and Atlas et al. (2013).

The following flow chart shows the connection of the regional OSSE system with the data from global OSSEs and the regional nature simulation.



The parent domain size for HWRF is configured to fit within the regional nature domain as shown in figure 3.

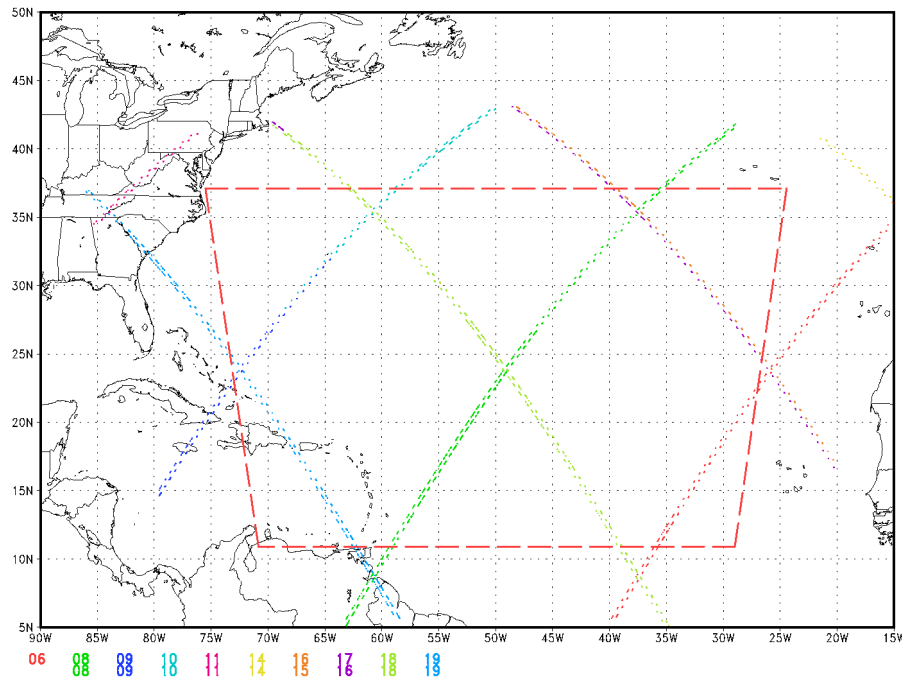


Figure 3: Domain configuration for the regional nature (outer frame) and HWRF simulations (red box) . Also shown is spatial distribution of simulated observations using the regional nature data. Different colors indicate different time period of the observations.

- **WISSCR Coherent** **Pulse Energy: 0.25 J**
 Aperture: 0.5 m (.79 m²)
 PRF: 10 Hz
 EAP: 1.98

- **WISSCR Double Edge** **Pulse Energy: 0.8 J (0.36 J @ 0.355 um)**
 Aperture: 0.5 m (.79 m²)
 PRF: 100 Hz
 EAP: 63.2 (28.44)

One figure of merit in making comparisons is the Energy Aperture Product (EAP). The two numbers on the EAP line for the OAWL and its DE companion system represent the EAP at the fundamental wavelength (1.06um) and at the tripled frequency wavelength of .355. It is clear that the WISSCR systems are smaller and require less platform power than the OAWL/DE. For example, the WISSCR final optics are a little over half the area of those of the OAWL/DE. However, the OSSE team considered this as acceptable for these OSSEs. The ultimate figure of merit may be costs and other factors not considered in this study. To be fair, any review of the results of this study should consider this basic resource difference between the two concepts since the data product coverage is different. This is particularly true of comparisons between the OAWL and coherent data products.

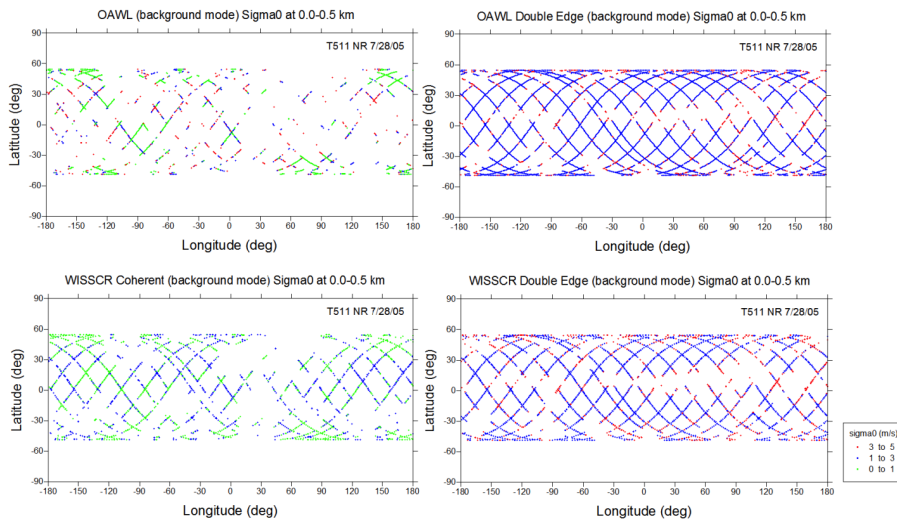
Ball Aerospace provided SWA, under an NDA, detailed system parameters and physics-based instrument model equations required to simulate the OAWL concept for OSSEs. The detailed system parameters for the WISSCR subsystems (coherent and DE) have been fully incorporated into SWA's simulation models for many years.

In addition to the instrument performance parameters addressed above, there were several key differences between the OAWL/DE and WISSCR data products that should be pointed out. The Ball instrument uses a laser for each of the two telescopes resulting in a continuous line of samples from both perspectives. The WISSCR concept cycles the beam from a single laser between the two perspectives. This results in a sampling gap equal in length to the sampled line.

The WISSCR mission concept used a 12 second dwell at each perspective. All samples during this 12-second period were processed into a single Line-of-Sight data product for data assimilation. The approximate length of this line of samples is 80 km. The timing of the forward and aft dwells was designed to obtain nearly spatially coincident overlays of both perspectives. Ball has chosen to operate in a manner similar to that proposed by the Japanese for the JEM/CDL mission. The continuous sampling from both perspectives allows for flexibility in post processing the data using various portions of the continuous line. For the OSSE simulations, we have produced LOS data products computed from 12 seconds of consecutive samples to allow comparisons between the OAWL and WISSCR data products (figure 4). However, the net result is that the OAWL/DE sampled data products are twice as numerous as those from the WISSCR. Consequently the impact through the Data Assimilation Systems may be enhanced for the OAWL system.

Given that NASA requested a study to give it guidance in planning a future space-based DWL mission, the disparities between the concepts described above are well within the same resource envelop provided by the ISS. It must be noted that the WISSCR concept could be altered somewhat to be more competitive by using multiple lasers in operation at the same time, increasing the size of the optics and using the more powerful direct detection laser proposed by Ball. However, it is the Team's judgment that such adjustments would result in only second order improvements in the data impacts.

Marine PBLs



Upper Troposphere

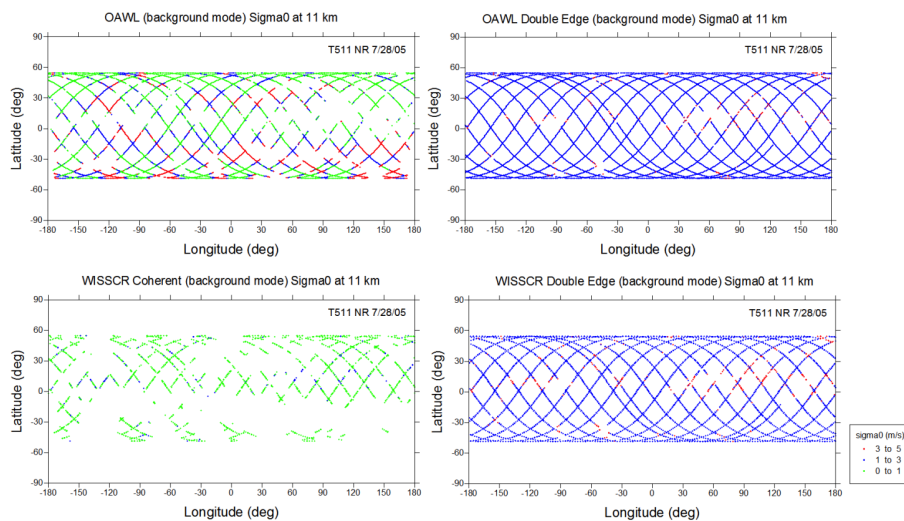


Figure 4. Sampling patterns for the LOS Doppler wind lidars within the Marine Boundary Layer (top set) and at 11km (bottom set) The sample size is a single LOS wind estimate every 80 km. The

uncertainty of the horizontal projection of the LOS velocity is noted with a color code shown in the lower right.

b. Wind observing system simulations

The Doppler Lidar Simulation Model

The Doppler Lidar Simulation Model (DLSM) is an evolution of existing Doppler lidar simulation models (<http://www.swa.com/ald/DLSM4.2/index.htm>; Wood et al., 2001; Wood et al., 2000; Emmitt and Wood, 1996) that are currently used to provide spaced-based Doppler lidar wind simulations for Observation System Simulation Experiments (Masutani, 2012; Riishojgaard et al., 2012; Riishojgaard et al., 2012). As shown in figure 5, the DLSM is a fully integrated Doppler lidar simulation model that produces simulated lidar winds and corresponding errors using either global or mesoscale atmospheric model wind fields. The DLSM can address various types of questions on the feasibility and optimal functionality of a space-based or airborne Doppler lidar system. The DLSM is also designed to address engineering trades, measurement accuracies (line of sight and horizontal wind vector), measurement representativeness, resolution and areal coverage.

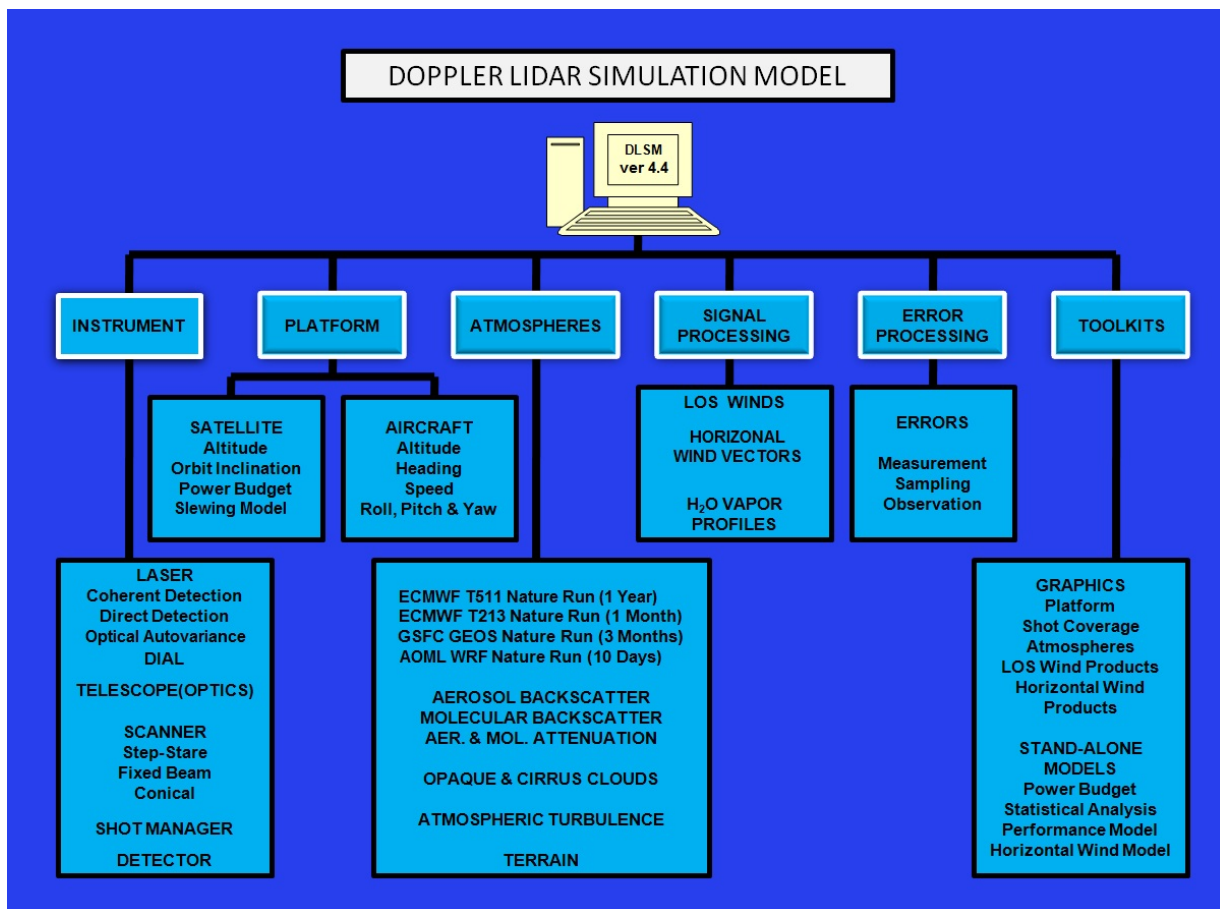


Figure 5 DLSM Block Diagram

The DLSM's atmospheric library contains many atmospheric databases including ECMWF T511, GSFC fvGCM and AOML WRF nature runs. These nature runs are used in liaison with SWA's Atmospheric Generator Model (AGM) to produce space-based views of clouds (opaque clouds, cirrus clouds and sub-visual cirrus), cloud optical properties, aerosol backscatter, molecular and aerosol attenuation, atmospheric turbulence and terrain.

Model Clouds

Perhaps the most critical aspect of the DLSM is the representation of clouds along the line of sight of each DWL "shot". For any given detection sensitivity of the DWL, clouds will determine how often observations are made throughout the troposphere. The challenge is to accomplish reasonable cloud representation of backscatter, attenuation, porosity, multi-layering and multiple-scattering effects using the grid-point values of idealized 4-D nature run model clouds.

The AGM cloud vertical structure model constructs a vertical profile of cloud information from the platform's viewpoint as shown in figure 6.

The AGM uses the following rules:

First, there has to be at least a 5 % cloud fraction for a cloud to be present at a given level. Second, if there is a cloud present, the cloud is considered opaque unless the liquid water content is less than an DLSM pre-set liquid water content threshold (currently set as 5%) and the air temperature is less than an DLSM pre-set air temperature threshold (currently set as 273K), then the cloud is considered to be a cirrus cloud. If the cloud is cirrus, the fractional cirrus cloud amount is not interpreted literally. Instead, the DLSM assumes 100% cirrus coverage and uses the fractional cirrus cloud amount to scale the cloud's optical depth. Thus all DWL "shots" would yield returns from cloud material and pass, attenuated, through to lower levels.

If the cloud is opaque and it is the first level that an opaque cloud is present, the DLSM uses the cloud's fractional amount to randomly decide the DWL's opportunity of getting a cloud return or an aerosol/molecular return. For subsequent cloud levels, the opportunity is dependent upon whether the cloud is contiguous or not. If contiguous, then only the additional amount of cloud in the DWL's view is randomly considered. If the cloud is non-contiguous, then the potential of cloud amount that is in the DWL view is randomly distributed in order to compute the amount of additional cloud present at the level.

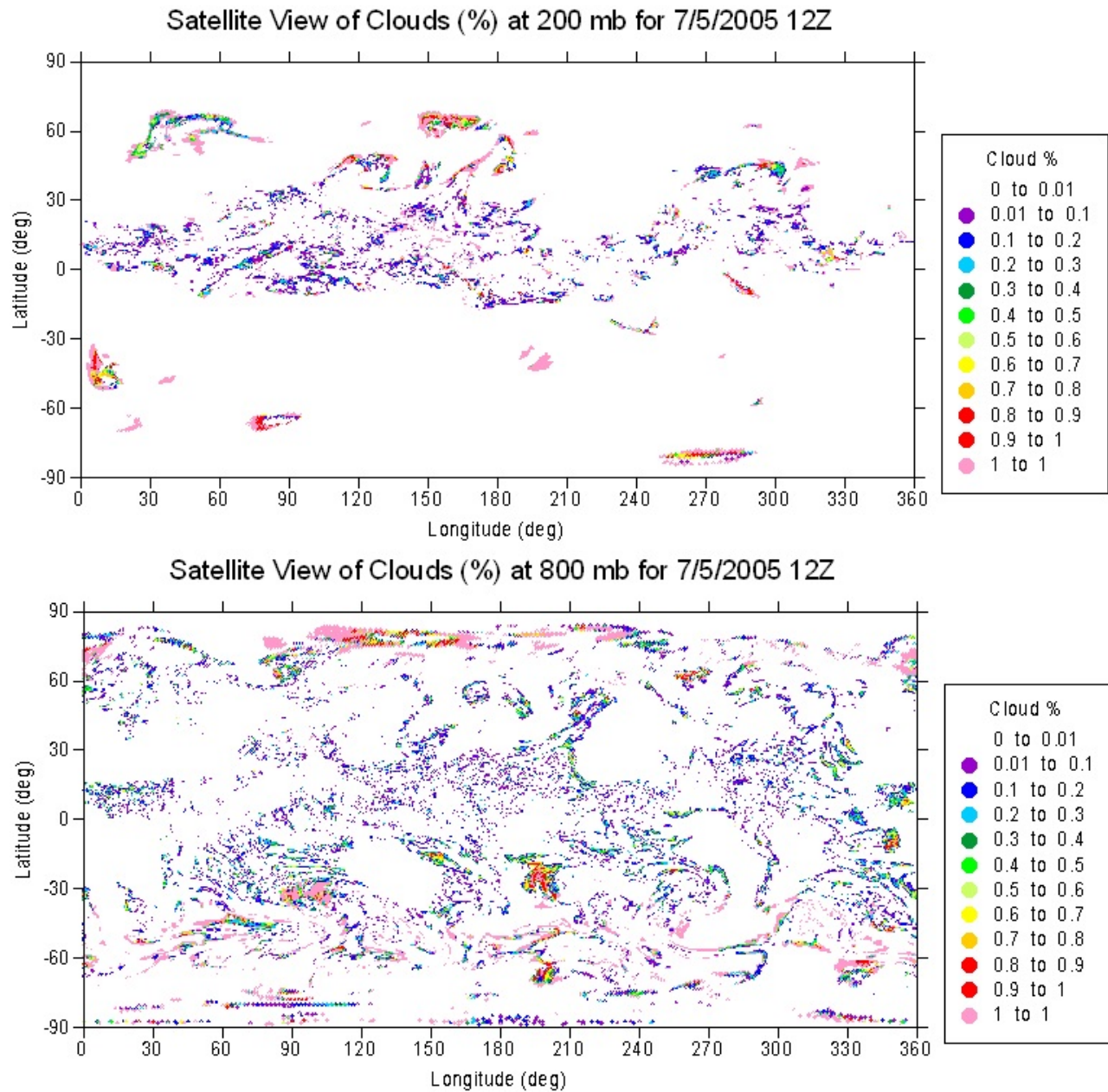


Figure 6. Satellite view of the Clouds for T511 Nature Run 7/5/2005 12Z at 200 and 800 mb respectively.

Aerosols

The DLSSM optical property models are currently based upon the Design Atmospheres for use in GTWS Concept Studies (Emmitt et al., 2001) provided by the Science Definition Team for the NASA/NOAA Global Tropospheric Wind Sounder. Having a common scattering target with internally consistent backscatter wavelength dependence enables meaningful "equal resource/equal target" comparisons of concepts that employ Doppler lidars. Aerosol backscatter from the atmosphere can vary over several orders of magnitude, and depends upon altitude,

latitude, and season. While this variability can be over space/time scales that are not readily modeled, the GLOBE, SABLE/GABLE backscatter surveys, and the AFGL FASCODE aerosol data bases provide a nearly consistent picture of backscatter climatology. The AGM provides background, enhanced and FASCODE optical property databases for 0.355 μm , 0.532 μm , 1.06 μm and 2.0518 μm DWL wavelengths. The DLSM can choose to use the median profiles or to use the median profiles with aerosol backscatter randomly distributed with lognormal variability as shown in the figure 7. The DLSM uses the same random data seed for an entire DWL "shot's" line of sight path.

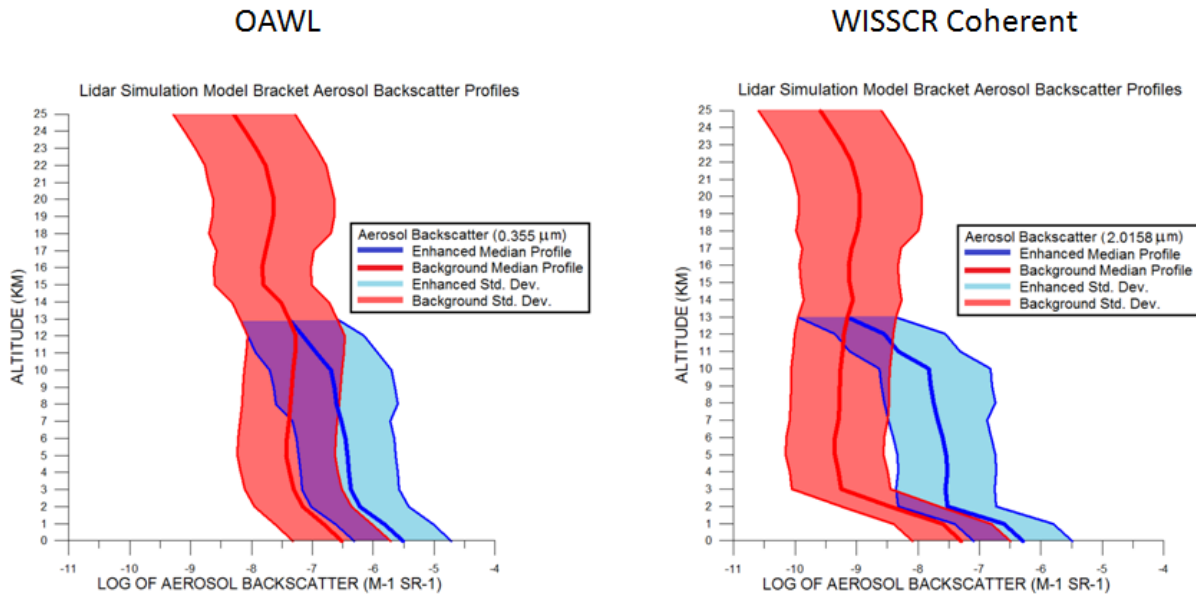


Figure 7. DLSM Probabilistic Aerosol Backscatter for OAWL and WISSCR. Background and Enhanced modes based upon the GTWS Concept Studies Design Atmospheres (Emmitt et al., 2001)

The AGM uses nature run humidity fields to organize in 3-D the aerosol scatter and backscatter optical properties. The OAWL/WISSCR simulations were generated for both background and enhanced modes for bracketing OSSEs. An example of the OAWL background mode aerosol backscatter organization using the ECMWF T511 Nature Run relative humidity fields for 500 and 1000 mb is shown in figure 8.

In past OSSE simulations of DWL observations, aerosol backscatter was taken from the PDF defined in the GTWS design reference atmospheres and assigned to a given level in the atmosphere. Since those backscatter profiles are composites constructed from sets of airborne backscatter observations and represent PDFs for different layers in the atmosphere they make no assumption regarding temporal or spatial correlation. For the current OSSE simulations, SWA proposed to redistribute the PBL driven aerosols in a more physically realistic vertical representation. Since the PBL is a 1st order concentrator of aerosols generated at the earth's surface and the new Nature Runs output a PBL depth, the distribution of aerosols is described by a well mixed layer of constant backscatter defined by the model's PBL with a rapid vertical

transition to the background (or enhanced) backscatter values. In the figure 9, the vertical backscatter distribution around the median for a 24 hour OAWL simulation using the T511 nature run is shown for the background and enhanced aerosol modes.

Global Aerosol Backscatter using Relative Humidity for Scaled Spatial Coherence

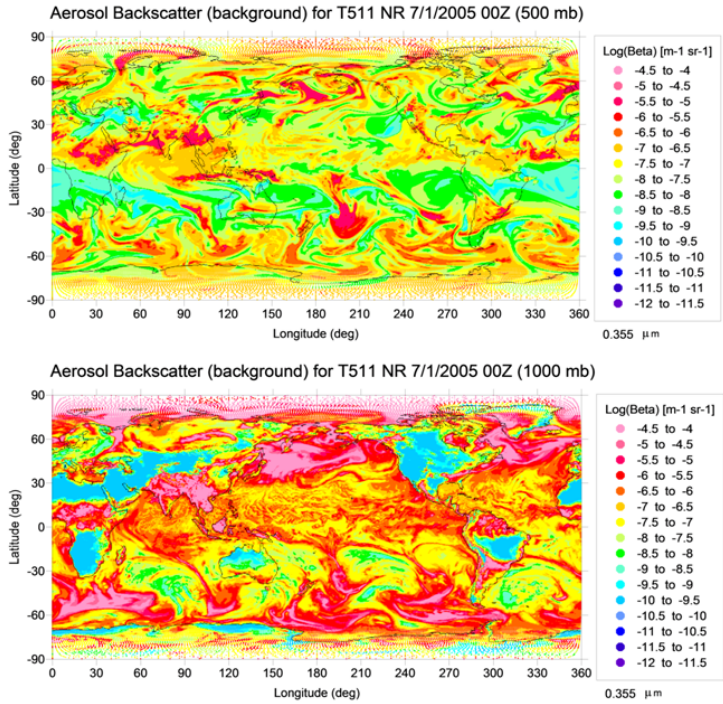


Figure 8. OAWL Background Mode Aerosol Backscatter organized by T511 Nature Run Relative Humidity for 500 and 1000 mb, respectively.

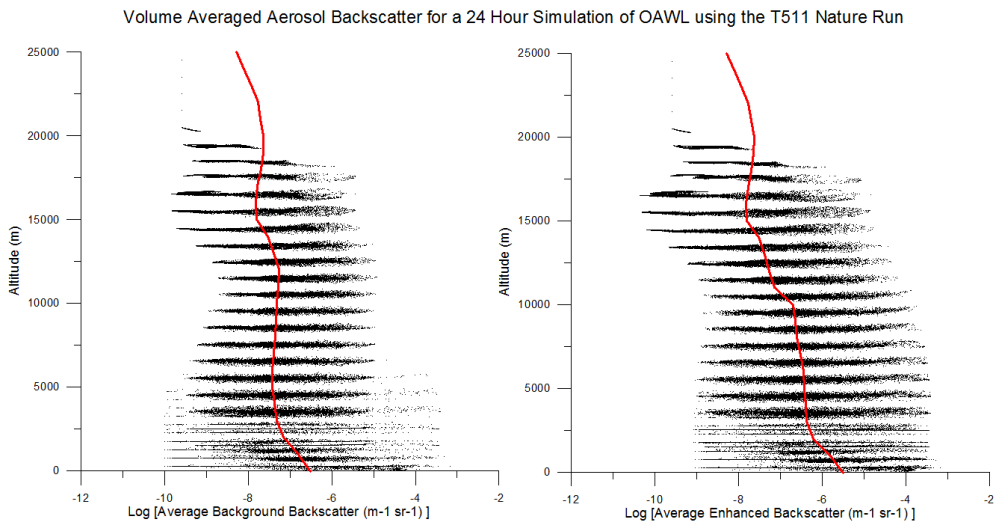


Figure 9. 24 hour Background and Enhanced Aerosol Backscatter distributions for the ECMWF T511 nature run.

Sub-grid Scale Variance

The DLSSM has two options for estimating the wind variance on the sub-grid scale of the model. The first method computes the wind variance on the grid scale (9 x 9 x 9) and then scaling the variance to smaller scales by the Von Karman relationship. The second method (used in the current simulations) represents the uncertainties by scaling them to 20 % of the mean model wind speed. Comparisons of the uncertainties with the NMC rawinsonde profiles suggest that the simulated variances using the 20 % rule are reasonable.

Simulated LOS vs Forward model LOS

SWA performed the following series of OAWL tests comparing the simulated LOS data with the forward model LOS data for 24 hours of the ECMWF T511 nature run:

- No sub-grid variance, no measurement uncertainty
- No sub-grid variance, measurement uncertainty
- Sub-grid variance, measurement uncertainty

As shown in figure 10, most of the simulated LOS variability from the nature run is due to measurement uncertainty. The sub-grid scale variance is being "beaten down" due to the large number of samples. Also shown is the good agreement between the DLSSM's simulated LOS winds to the nature run when no variability is included.

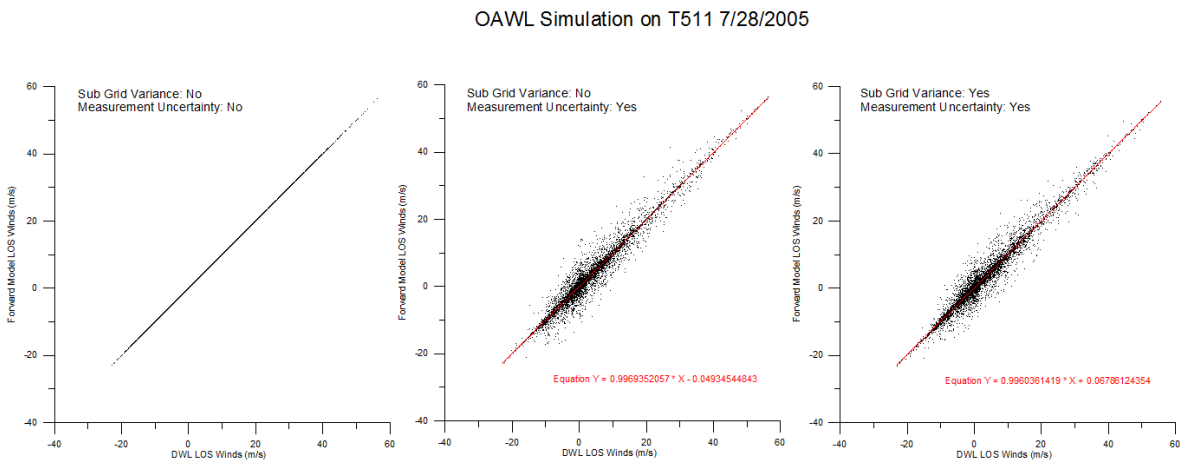


Figure 10. Comparison of simulated LOS winds for OAWL to T511 nature run LOS winds.

- a. No sub-grid variance, no measurement uncertainty
b. No sub-grid variance, measurement uncertainty.
c. Sub-grid variance, measurement uncertainty

c. Simulation of orbit and shot time series

With some assistance from Ball Aerospace, SSSO used the AGI Satellite Tool Kit (STK; see <https://www.agi.com>) to generate time series of lidar shot locations. STK was hosted on an Apple MacPro workstation running the OS X operating system and the Parallels Desktop virtual

machine software (see <http://www.parallels.com>), which in turn was used to run the Microsoft Windows XP operating system. This system was inherited from the Sensor Web project (Talabac et al 2011), and was originally intended to generate orbit and shot calculations. A customized orbit/shot scenario was created, using the International Space Station (ISS) with two look angles (forward and aft) on the port side of the station. A shot frequency of 100 Hz from both shot angles was selected, with azimuth angles of 45 and 135 degrees and an elevation angle of 47 degrees. A day/night flag was also added to the output at the request of SWA.

STK was run in batch mode to produce two sets of shot time series: one for the fvGCM Nature Run (24 September to 23 October 1999), and one for the T511 Nature Run (29 July to 11 August 2005). Script development was required to automate STK for these tasks. Significant run-time problems were encountered during time series generation: STK proved to be slow and unstable, and required frequent manual intervention to restart calculations. In addition, the MacPro workstation occasionally rebooted or experienced fatal memory errors, which were attributed to failing hardware. [This system has since been decommissioned and excessed.]

Once the data were collected from STK, it was post-processed to mimic the specific lidars. Both the OAWL and companion double edge lidar were assumed to have 100 Hz frequencies but with alternating forward/aft look angles, i.e., each look angle had an effective frequency of 50 Hz. For the WISSCR coherent and double edge modes, frequencies of 10 Hz and 100 Hz were used respectively. Both used a 12 second dwell time (laser pointing out of single shot angle) and a 1.3 second gap (no observations as laser switches between shot angles). Due to the quantity of the STK data, the post-processing software required several optimization rewrites. [The first version took over 2 wall clock hours to process 24 hours of STK data; this was ultimately reduced to 20-30 wall clock minutes, and parallelization was added.]

These post-processed data were ingested into the DLSM by SWA to produce synthetic LOS lidar observations. Two sets of observations were produced using the background and enhanced aerosol models. Data from the fvGCM were used to derive 2-D horizontal wind vectors (required by GEOS-DAS). FvGCM-based observations were only generated from 24 September to 9 October.

d. Quality control and assignment of observation errors

The synthetic lidar observations produced by the DLSM are designed to be *realistic* and faithful to real-world performance. A consequence is that the observations have a range of accuracies as a function of atmospheric conditions, with some observations containing gross errors unsuitable for assimilation. It is therefore necessary to apply quality control checks. In addition, the data assimilation systems require a reliable estimate of *observation error* σ_o , which includes not only the *measurement error* σ_m but also the *representativeness error* σ_r relating the observation sampling to the grid resolution of the data assimilation system. The formal equation combining these errors (assuming independence between σ_m and σ_r) is:

$$(1) \quad \sigma_o^2 = \sigma_m^2 + \sigma_r^2.$$

The DLSM provides σ_m values unique to each observation but neither σ_o nor σ_r .

Two separate quality control thresholds and σ_o assignment procedures were employed depending on the OSSE system. For the GEOS-DAS/fvGCM, quality control thresholds and σ_o values were made proportional to rawinsonde values in the following method:

- Rawinsonde σ_o values were set by interpolating GEOS-DAS standard lookup table values at standard pressure levels to the observation positions.
- Rawinsonde σ_m was assumed to equal the WMO standard value of 0.5 m/s for all levels.
- Equation 1 was used to determine a numerical value of rawinsonde σ_r .
- Lidar σ_r (horizontal wind) was set to 75% of the rawinsonde σ_r . This percentage is a crude way of accounting for higher sampling of an atmospheric volume by a lidar versus a rawinsonde.
- Two lidar σ_o tiers were established. Tier 1 set lidar σ_o (horizontal wind) equal to the rawinsonde σ_o , while Tier 2 set lidar σ_o (horizontal wind) to twice that value.
- For a given tier, Equation 1 was used to estimate a lidar σ_m horizontal wind threshold given the σ_o and σ_r .
- The horizontal wind σ_m was divided by cosine of 48.46 degrees to transform it into an appropriate LOS threshold Figure 11 shows the LOS σ_m thresholds as a function of pressure.
- The LOS tier σ_m threshold was compared to the forward and aft LOS σ_m values for a 2D horizontal wind observation. If both LOS σ_m were less than the Tier 1 threshold, then the observation was put in the Tier 1 bin. Otherwise, if both LOS σ_m were less than the Tier 2 thresholds, then the observation was designated Tier 2. Otherwise, the observation was rejected.

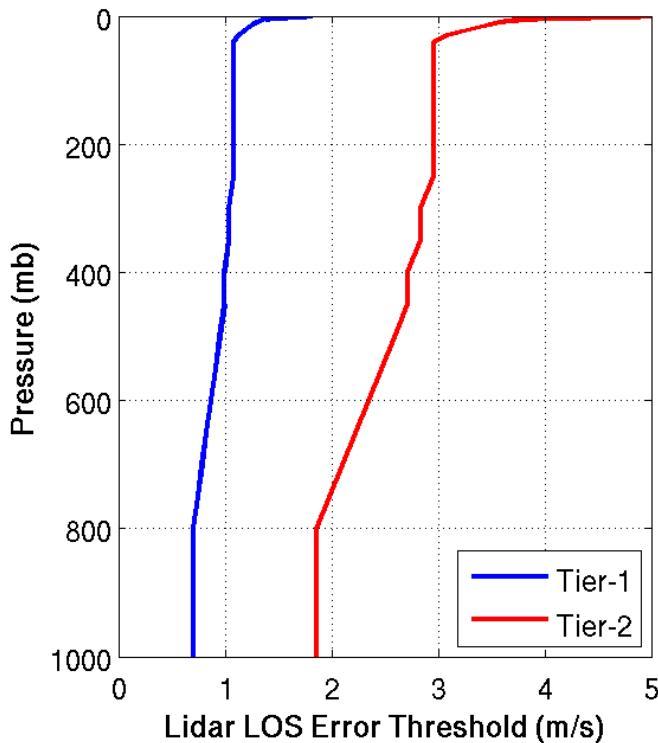


Figure 11: Lidar LOS σ_m thresholds for Tier 1 and Tier 2 as a function of pressure.

The tables below give a breakdown of the horizontal wind vector observations by lidar and model and the assigned tiers. Note that the WISSCR coherent lidar produces roughly an order of magnitude fewer observations than the other lidars, and the double edge lidar observations have higher measurement errors with few qualifying as Tier 1 (none in the case of the WISSCR double edge).

OAWL HWVs: 1383913 Tier 1 Subset: 593730 (42.9%) Tier 2 Subset: 451379 (32.6)	DE HWVs: 2295609 Tier 1 Subset: 77741 (3.4%) Tier 2 Subset: 2011274 (87.6%)
WISSCR coherent HWVs: 148388 Tier 1 Subset: 100756 (67.9%) Tier 2 Subset: 38892 (26.2%)	WISSCR DE HWVs: 1012038 Tier 1 Subset: 0 (0%) Tier 2 Subset: 901289 (89.1%)

Summary statistics for lidar horizontal wind observations assuming background aerosol model.

OAWL HWVs: 1448290 Tier 1 Subset: 748075 (48.0%) Tier 2 Subset: 476125 (30.6%)	DE HWVs: 2178510 Tier 1 Subset: 62637 (2.9%) Tier 2 Subset: 1914173 (87.9%)
WISSCR coherent HWVs: 295345 Tier 1 Subset: 168612 (57.1%) Tier 2 Subset: 108514 (36.7%)	WISSCR DE HWVs: 957346 Tier 1 Subset: 0 (0%) Tier 2 Subset: 854615 (89.3%)

Summary statistics for lidar horizontal wind observations assuming enhanced aerosol model.

After binning, the observations were encoded in BUFR format as if they were rawinsondes, with a limit of 70 observations per “rawinsonde profile.” Profiles were then assigned σ_o corresponding to their Tier.

While it is recognized that the DLSM simulation provides very detailed information about the expected quality of the observations generated, using this directly to assign observation error variances in the assimilation did not lead to a positive impact of the observations in the OSSEs performed by JCSDA using the NCEP Global Forecast System (section 7). It was therefore decided to simply use the GFS preassigned error variances used for radiosonde observations, which vary by vertical level only, for all Lidar data, irrespective of assumed or simulated quality. The main reason is that since the background error is imperfectly known, even very accurate information about the observation error may lead to imperfect results as was found here. Generally, optimal results are found when the analysis weights (related to the ratio between background error and observation error) are optimal, and it is therefore often counterproductive to model only one of the two error terms in great detail while holding the other fixed.

In the regional data assimilation using the HWRF model and GSI with OAWL and WISSCR simulated observations that were based on the regional nature simulation, the observation errors as specified in the simulated observations were utilized. Also, the gross error of 2.5 ms^{-1} was used in GSI for the lidar observation type.

5. Data Product Evaluation

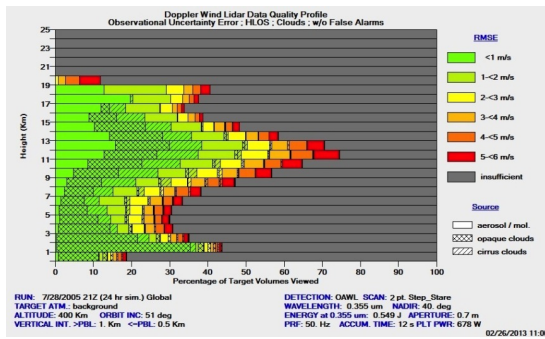
For more than 20 years, DWL OSSE efforts have involved a “pre-OSSE” evaluation of the simulated data products. One tool in summarizing the vertical coverage of the simulated wind products is the “Performance Diagram” shown in figures 12 through 19. While this pre-OSSE provides insight to the number, quality and vertical distribution of lidar wind observations, it does not, and should not, be seen as an end product. The end product is a statement on the impact that these observations would have on forecasts. On the other hand, these performance diagrams serve as a good way to compare the quality and distribution of LOS winds from differing DWL concepts. In this study, we proposed to evaluate the differences in the data products simulated for OAWL and WISSCR before committing to an extensive series of OSSEs. If there were insignificant differences in the data going into the DAS, then the argument for more OSSEs would have been weak. However, as shown below, this was not the case and the new series of OSSEs were required. In mid course of this project, the OSSE team decided to use the “bracketing” approach to deal with the fidelity of assigning aerosol opportunities around the globe in a realistic manner. Thus data was simulated for two series of OSSEs; one with the background mode described in the previous section and one with the enhanced mode.

The LOS performance diagram displays the percentage of time that a lidar system can make useful measurements in terms of sufficient aerosols, molecules, clouds and cirrus clouds in the vertical for each attempted profile. The chart also reflects the percentage of no returns due to opaque clouds. In figures 12 - 19, the global vertical distribution of data products and their quality are summarized for each subsystem studied for both background and enhanced modes and for with and without clouds in the simulation.

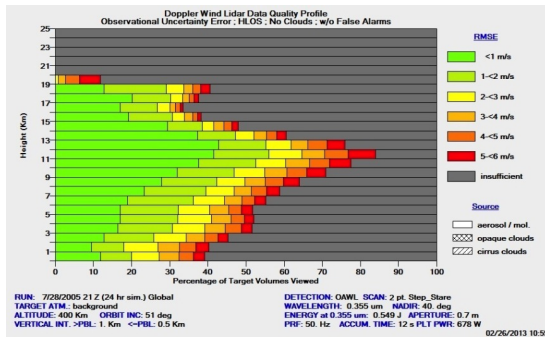
The primary comments we can make regarding the Pre-OSSE “Performance Diagram” shown in figures 12 -19 are:

- The Energy Aperture Products (EAP) for the OAWL and companion DE detector are significantly higher than those for the WISSCR concepts. This disparity should be taken into consideration when making comparisons between the OAWL and WISSCR_coherent instruments but it does not offset other advantages of the OAWL technique.
- The vertical coverage of useful quality “aerosol winds” for the OAWL system is much greater than that for the WISSRC_coherent system. This is due not only to the larger EAP for OAWL but the fact that, as a direct detection technique, the falloff in velocity measurement precision is not as precipitous as in the case of coherent detection. Another way to express this advantage is that OAWL can return an observation with 3m/s (or greater) precision when aerosols are more scarce than the design concentrations while the coherent system would not report an observation of less than 1.5m/s once the concentrations fell below a design threshold.

- The vertical coverage of the DE systems in the mid and upper troposphere is comparable for both mission scenarios. This fact explains why the team chose to focus on comparing just the aerosol subsystems in the OSSEs.
- The coherent system (WISSCR_coh) is the better PBL wind observing system while the OAWL provides more quality aerosol winds in the mid and upper troposphere given. The coherent detection technique remains superior to the OAWL technique for producing high precision measurements in the presence of clouds and sufficient aerosols (primarily in the PBL).

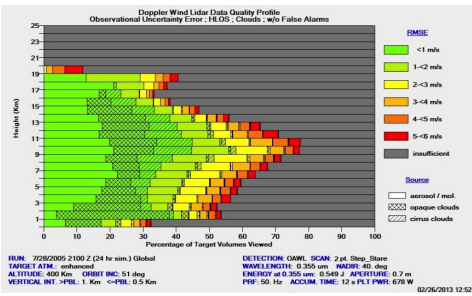


OAWL with Clouds
Backscatter Mode: Background

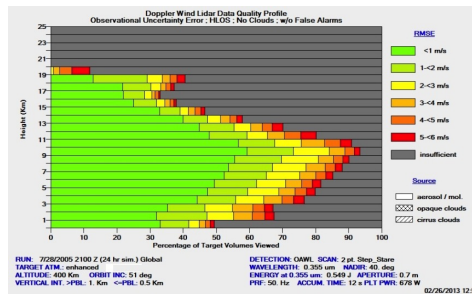


OAWL without Clouds
Backscatter Mode: Background

Figure 12. The top panel displays a performance profile for the **OAWL background aerosol** detection baseline system described in section 4.0. These plots should be viewed as stacked histograms of horizontally projected observational uncertainty (measurement error σ_m) along the LOS. The color bars express both the % of all attempts at a given level that met various values of σ_m . The uncertainty estimates include the effects of aerosols, sample scale turbulence, opaque clouds and cirrus clouds. The bottom panel is a performance profile with a “no cloud” assumption which illustrates the impact of clouds on the data coverage.

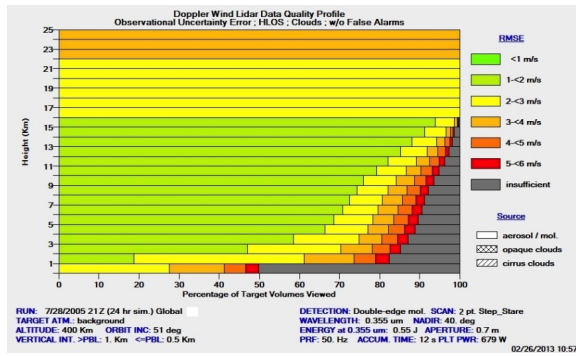


OAWL with Clouds
Backscatter Mode: Enhanced

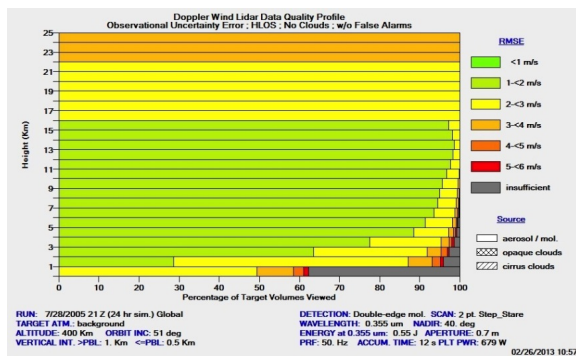


OAWL without Clouds
Backscatter Mode: Enhanced

Figure 13. Same information as explained in figure 12 caption except for OAWL enhanced aerosol mode.

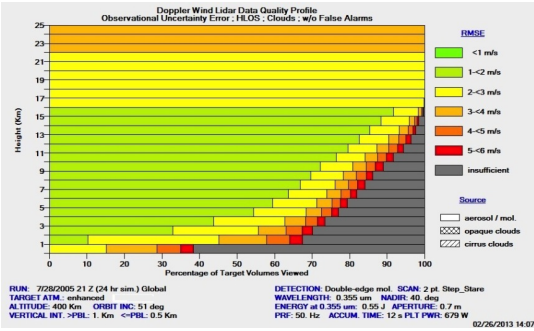


OAWL Double Edge with Clouds
Backscatter Mode: Background

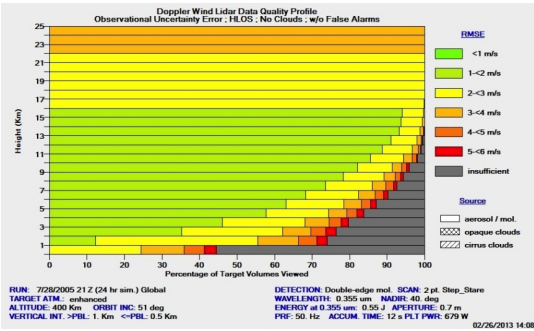


OAWL Double Edge without Clouds
Backscatter Mode: Background

Figure 14. Same information as explained in Figure 12 caption except for OAWL Double Edge when the background aerosol is present.

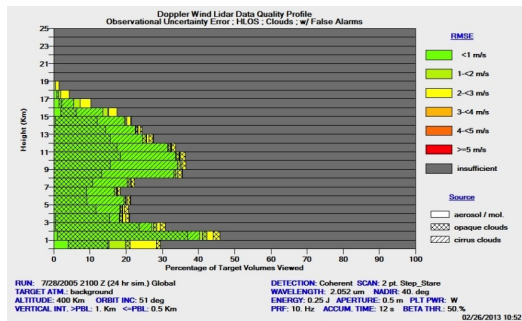


OAWL Double Edge with Clouds
Backscatter Mode: Enhanced

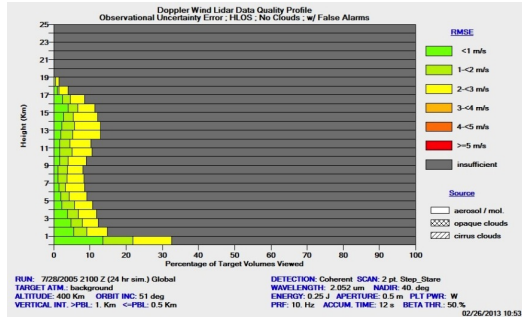


OAWL Double Edge without Clouds
Backscatter Mode: Enhanced

Figure 15. Same information as explained in Figure 12 caption except for **OAWL Double Edge** when the enhanced aerosol is present.

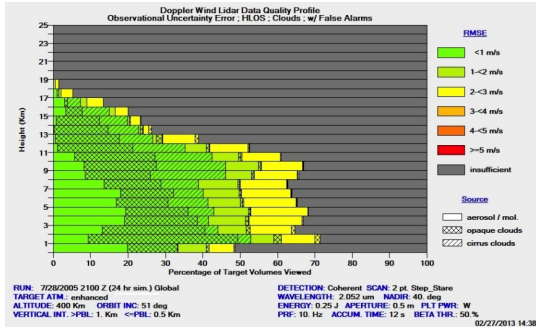


WISSCR Coherent with Clouds
Backscatter Mode: Background

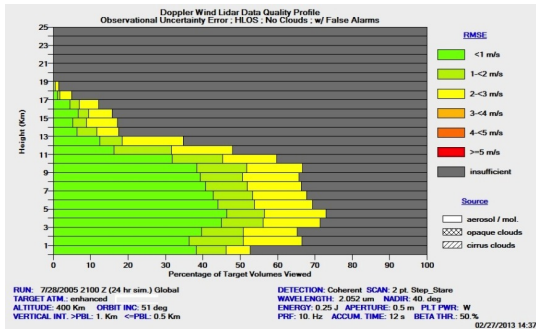


WISSCR Coherent without Clouds
Backscatter Mode: Background

Figure 16. Same information as explained in Figure 12 caption except for **WISSCR coherent** when the background aerosol is present

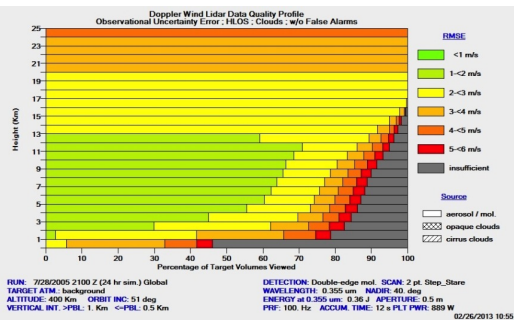


WISSCR Coherent with Clouds
Backscatter Mode: Enhanced

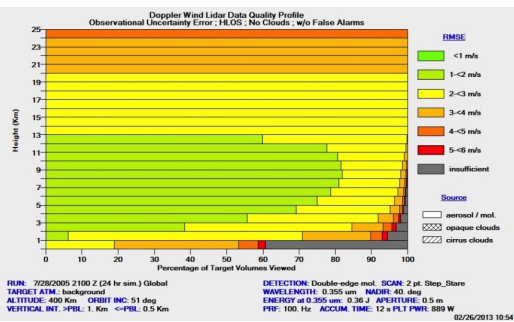


WISSCR Coherent without Clouds
Backscatter Mode: Enhanced

Figure 17. Same information as explained in Figure 12 caption except for WISSCR coherent when the enhanced aerosol is present.

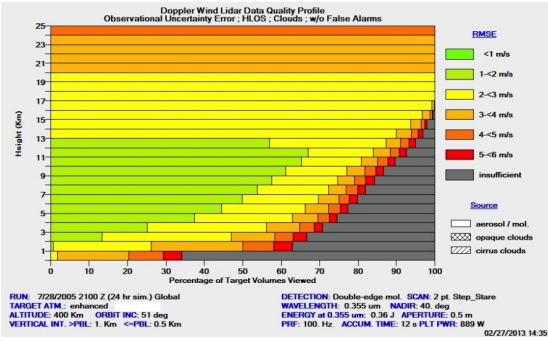


WISSCR Double Edge with Clouds
Backscatter Mode: Background

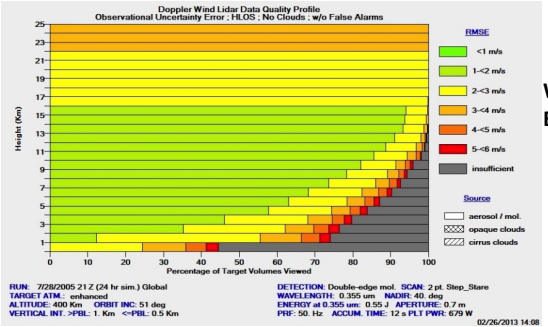


WISSCR Double Edge without Clouds
Backscatter Mode: Background

Figure 18. Same information as explained in Figure 12 caption except for WISSCR Double Edge when the background aerosol is present.



**WISSCR Double Edge with Clouds
Backscatter Mode: Enhanced**



**WISSCR Double Edge without Clouds
Backscatter Mode: Enhanced**

Figure 19. Same information as explained in Figure 12 caption except for **WISSCR Double Edge when the enhanced aerosol is present.**

6. GEOS-5 DAS/fvGCM results

A set of five OSSEs were performed by SSSO for the period of 24 September to 9 October, with 5-day forecasts produced daily at 00 UTC. The experiments are:

- Control (CNTL): Assimilates radiosondes, surface observations, aircraft reports, ship reports, satellite retrievals, perfect QuikSCAT, and GOES-R cloud drift winds.
- OWLB: Assimilates Control observations plus OAWL and DE lidars (both tiers) using background aerosol model.
- OWLE: Similar to OWLB but uses enhanced aerosol model.
- WISB: Assimilates Control observations plus WISSCR coherent and DE lidars (both tiers) using background aerosol model.
- WISE: Similar to WISB but uses enhanced aerosol model.

To assess forecast quality, anomaly correlations (AC) of select variables were calculated on the full set of forecasts out to 5 days. Figures 20 and 21 show the AC values for 500 mb geopotential heights for the northern and southern extratropics, defined as the area from 20 to 80 degrees latitude. Figures 22 and 23 show corresponding AC values for mean sea level pressure. In general, the AC values for the Control experiment (no lidar assimilation) either matches or exceeds the values for the remaining experiments. Similar results (not shown) were obtained when looking at RMSE scores. These results are surprising, and conflict with earlier OSSE findings summarized in Atlas and Riishojgaard (2008). However, the earlier OSSE with the fvGCM utilized a fully validated OSSE system and assimilated a swath rather than a line of data. To explore this issue further, two additional idealized experiments were performed:

- WISP: Assimilates Control observations plus “perfect” wind profiles at latitude/longitude coordinates of WISSCR observations. The wind profiles are interpolated directly from the fvGCM and no errors are inserted. This experiment is intended to assess sensitivity to data quality.
- WISS: Assimilates Control observations plus a *swath* of “perfect” wind profiles at locations derived from 7 different azimuth angles on the port side of the ISS. Wind profiles are again interpolated directly from the fvGCM. This experiment is intended to assess sensitivity to data coverage.
- Both experiments were run for 6 days (24-29 September), and both had assigned errors equal to those for rawinsondes.

Figures 24 and 25 show the 500 mb geopotential height AC scores in the extratropics, while figures 26 and 27 show the AC scores for mean sea level pressure. The WISS results (using a swath of 7 azimuth angles) are better than WISP (using WISSCR shot locations), and show the importance of greater horizontal coverage. However, WISS still only shows modest improvement over the Control run in the Northern Hemisphere extra-tropics, and also shows degradation of forecast quality in the Southern extra-tropics. Similar results (not shown) are indicated with RMSE scores. These results again conflict with earlier OSSE results, and indicate that the deficiencies of the GEOS-5/fvGCM OSSE system do not permit meaningful experiments. We reluctantly conclude that the GEOS-5DAS/fvGCM cannot be used for OSSEs without significant development and validation. Our evaluation of the OAWL and WISSCR technologies will thus be based on the NCEP GFS/T511 and HWRF/ARW-T511 systems instead.

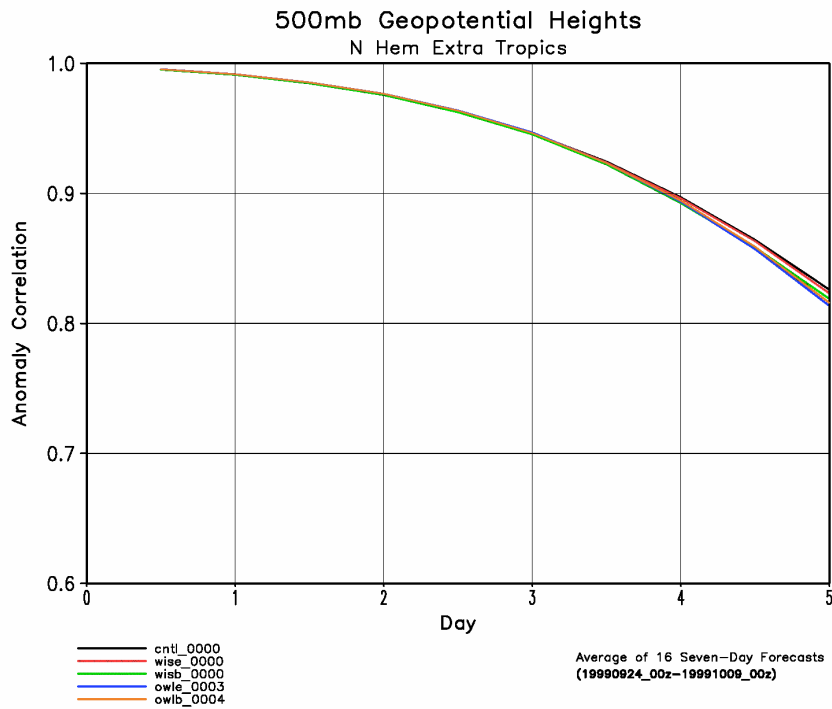


Figure 20. 500 mb geopotential height anomaly correlations for 20 to 80 degrees North latitude for Control and lidar experiments.

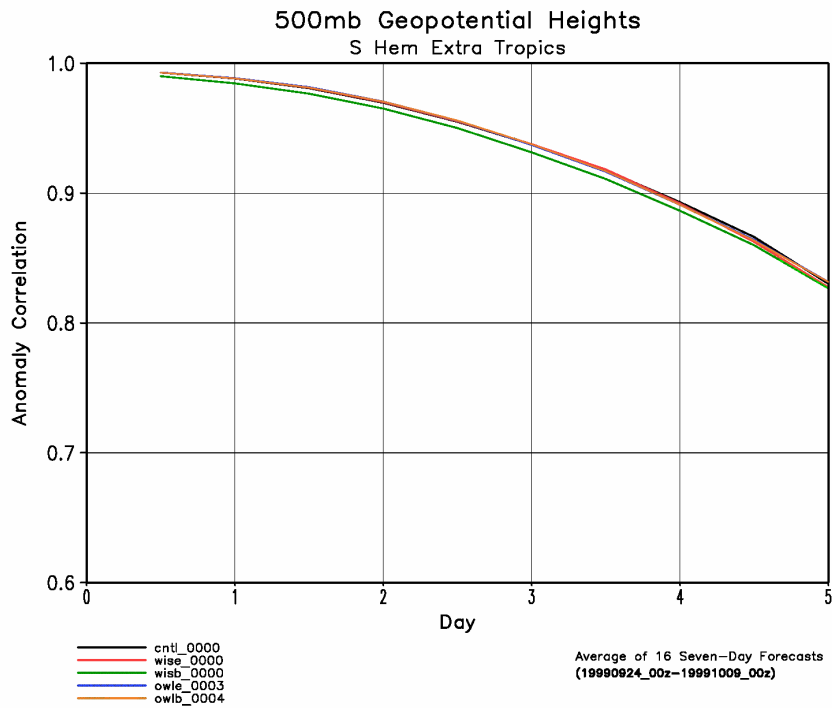


Figure 21. 500 mb geopotential height anomaly correlation for 20 to 80 degrees South latitude for Control and lidar experiments.

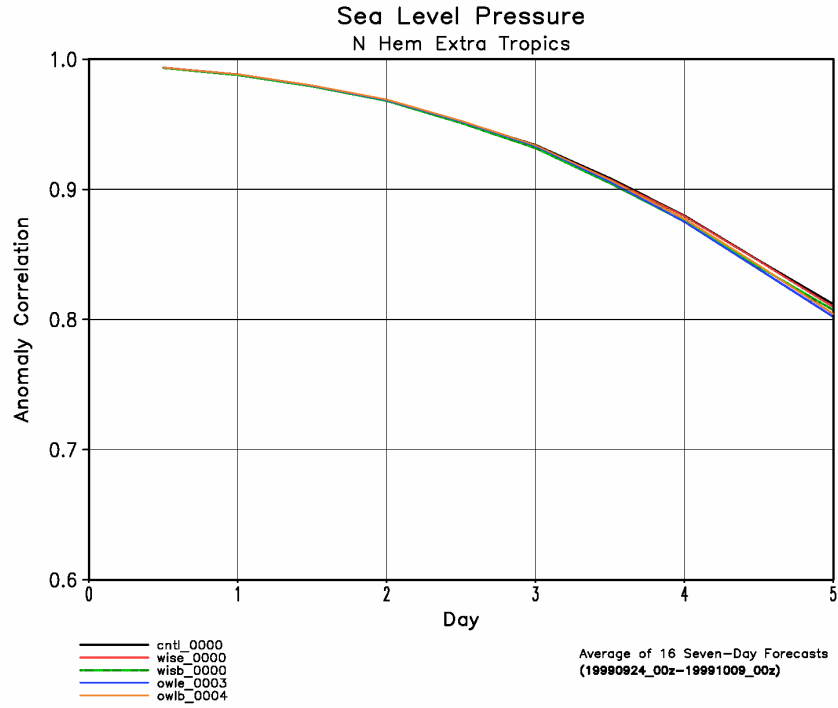


Figure 22. Mean sea level pressure anomaly correlation for 20 to 80 degrees North latitude for Control and lidar experiments.

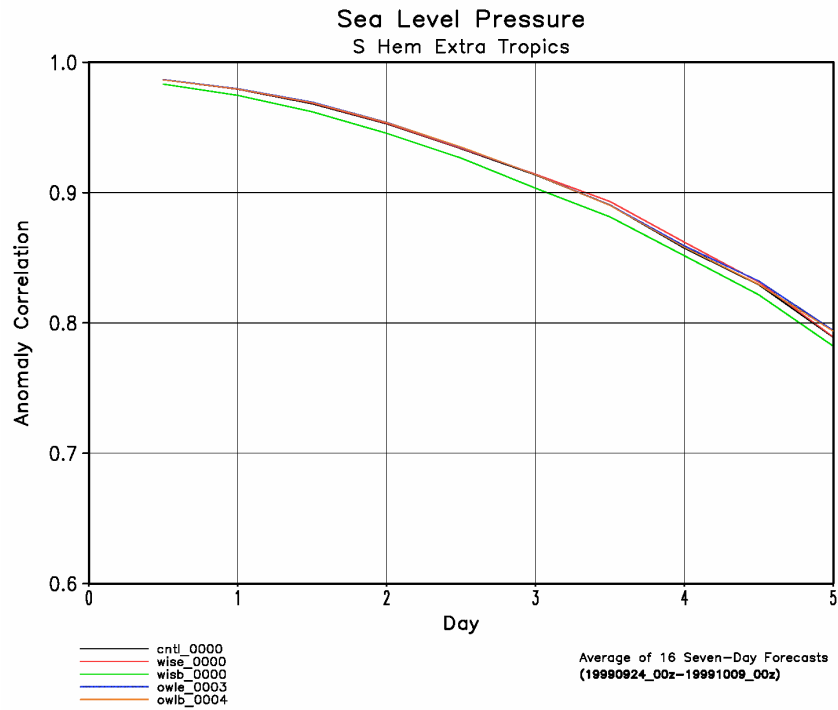


Figure 23. Mean sea level pressure anomaly correlation for 20 to 80 degrees South latitude for Control and lidar experiments.

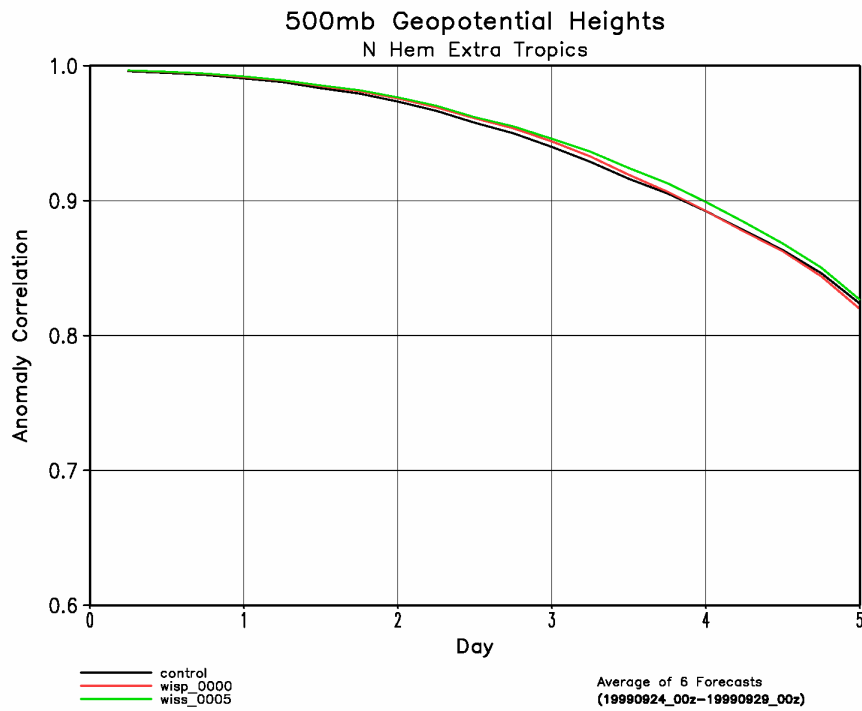


Figure 24: 500 mb geopotential height anomaly correlation for 20 to 80 degrees North latitude for Control and idealized experiments.

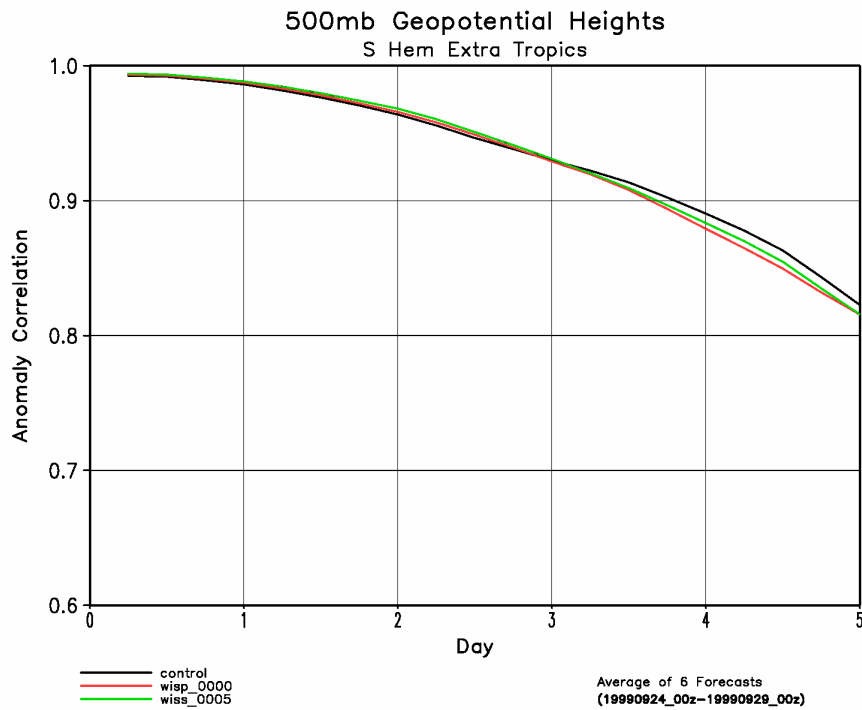


Figure 25: 500 mb geopotential height anomaly correlation for 20 to 80 degrees South latitude for Control and idealized experiments.

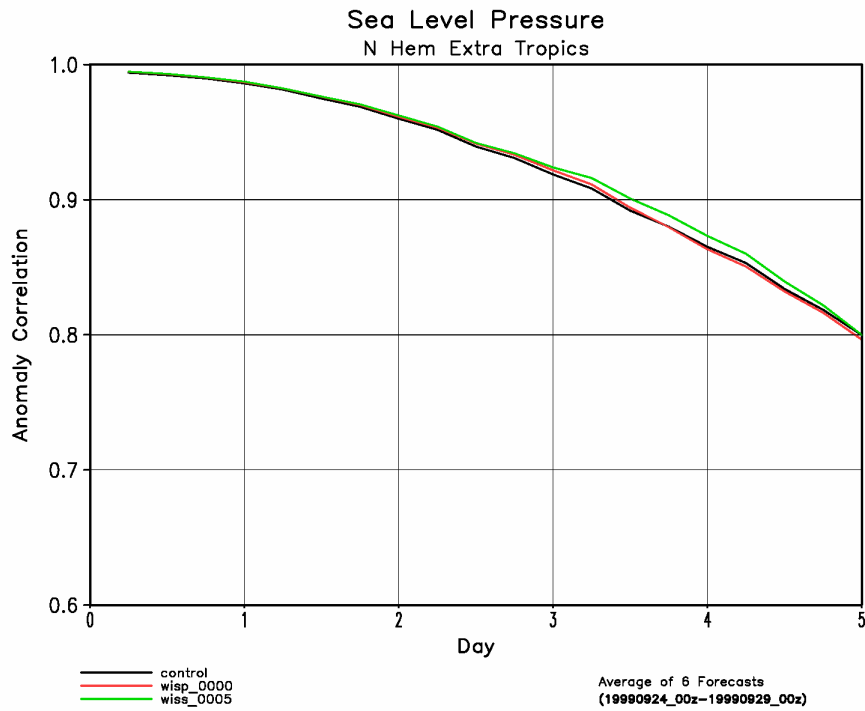


Figure 26: Mean sea level pressure anomaly correlation for 20 to 80 degrees North latitude for Control and idealized experiments.

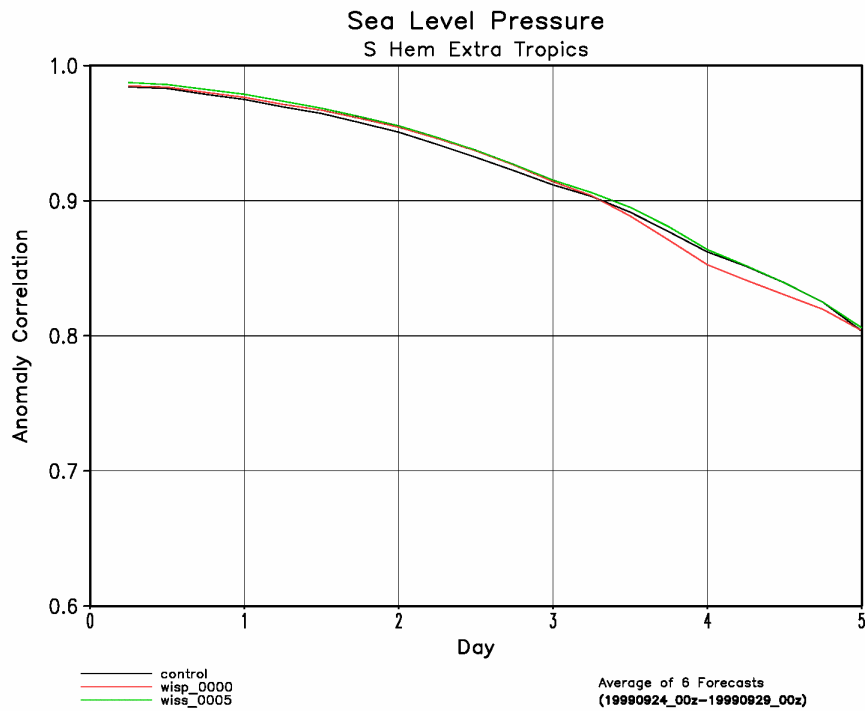


Figure 27: Mean sea level pressure anomaly correlation for 20 to 80 degrees South latitude for Control and idealized experiments.

7. NCEP GFS/ECMWF T511 results

To assess the impact of the simulated lidar wind data from the different lidar observing systems (OAWL and WISSCR_COH), two sets of experiments were conducted (Figure 28): first, a cycling assimilation experiment for almost one-month period from 2818 UTC on 28 July to 0000 UTC on 24 August 2005, in which the GSI assimilation system is used for the analysis component and the GFS forecast model is used for the 6-h forecast component. And then due to limited computer resources, one forecast a day (only from the corresponding analysis at 0000 UTC with the GFS forecast model) was run out to 168 hours (or 7 days). The details of the experimental design are described as follows.

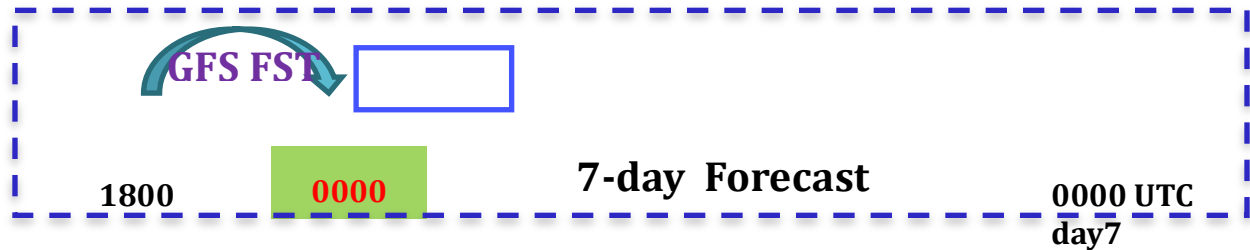


Fig. 28 The design of the impact experiment assimilating without/with lidar wind data in the lidar OSSE.

Three experiments have been carried out in each set: (1) CTRL: A control run in which all the simulated equivalents of observations (both conventional and space-based used operationally by NCEP in 2012; (2) OAWL: Same as CTRL, but adding OAWL lidar wind data; (3) WISSCR_COH: Same as CTRL, but adding WISSCR coherent lidar wind data.

The observation system simulation experiments were conducted to compare the respective impacts of using the simulated lidar data from the OAWL and WISSCR_COH. The preliminary results are analyzed in this section as follows. First we discuss the impact of the different sets of lidar wind data on analyses for the complete one-month assimilation period. In the second subsection, we perform the 168-h forecasts where the analysis from each run serves as the forecast initial state. The impact of lidar data on forecasts is assessed based on objective statistical measures to verify forecasts initialized with either OAWL or WISSCR_COH and without lidar data (as the CTRL). In this OSSE, forecast impact comparisons will be presented for assimilating the operational data to a benchmark or Control experiment. The impact on the quality of the GFS forecasts from assimilating the different sets of lidar data is explored in detail.

The primary fields used for the verification are the tropical winds and the extratropical 500-hPa geopotential heights. Several objective statistical measures to verify forecast quality are commonly used. Most popular among these are the Root-Mean Squared Error (RMSE) and the Anomaly Correlation Coefficient (ACC) of forecasts against verifying analyses. In this assessments both analyses and forecasts are verified against the Nature Run for each experiment, using the NCEP operational verification package. Since the Nature Run from the ECMWF was performed at a resolution of T511L64 and the lidar OSSE was carried out at a resolution of T382L64, both datasets were reduced to a 2.5° by 2.5° horizontal resolution before calculating the RMSE and anomaly correlations with this package. The extratropical verification is done for the latitudinal bands of 20°-80° in each hemisphere, while the tropical

verification is done in the band from 20°N to 20°S. More details about the NCEP verification package can be found on the NCEP web site

7.1 TROPICAL WINDS

In this section, the comparison of vector winds from analyses and forecasts with respect to the Nature Run is investigated first. Because of the OSSEs were performed for lidar wind observations, the RMSE of the wind vector analyses will be investigated mainly. Here RMSE is defined according to the WMO standard using the following equation:

$$RMSE = \sqrt{\frac{1}{n} \sum_{n=1}^N (F_n - A_n)^2} \quad (2)$$

where F is the analysis or forecast value of the parameter under investigation, A is the true atmospheric state (from the Nature Run), and N is the total number of points in a temporal or spatial domain or a spatial-temporal combined space. The summation is over all gridpoints inside the verification area. In the case of wind vector verification, the summation in the numerator contains two terms – the zonal and the meridional wind components.

As an example of lidar observation impact, a time series of RMSE from the tropical wind vector analysis is displayed in Figure 29 for different pressure levels, i.e., RMSE on P200 hPa presents a comparison of wind vector RMSE for three OSSE experiments (CTRL, OAWL and WISSCR_COH) at 200 hPa over the tropical regions. Compared with the CTRL, a positive impact from lidar data on the analysis is clearly seen. The temporal mean, taken over all 20 cases displayed, is shown in the middle column of the legend in each figure. In order from worst to best, the time-averaged RMS error of the tropical 200 hPa winds of the three experiments are: CTRL (3.971 ms⁻¹) > WISSCR_COH (3.788 ms⁻¹) > OAWL (3.300 ms⁻¹). Similar results can be found at 850 hPa.

Figure 30 shows the time series of RMSE from the wind vector analysis against the Nature Run for pressures from 1000 hPa to 10 hPa in the tropics. The biggest RMSE value from the CTRL run (showed in the Up-Left panel) appears at the higher levels between 50 to 10 hPa. The differences between the lidar runs (OAWL and WISSCR_COH) and the CTRL are calculated and shown as well. The green areas denote a positive impact of the wind lidar observations, or in other words that the wind vector RMSE from the lidar run is smaller than that from the CTRL. On the other hand, red areas denote a negative impact of the lidar data. It is clearly seen that most areas are green. Meanwhile, as expected, the largest positive impact of the lidar data appears at the higher levels for OAWL experiments.

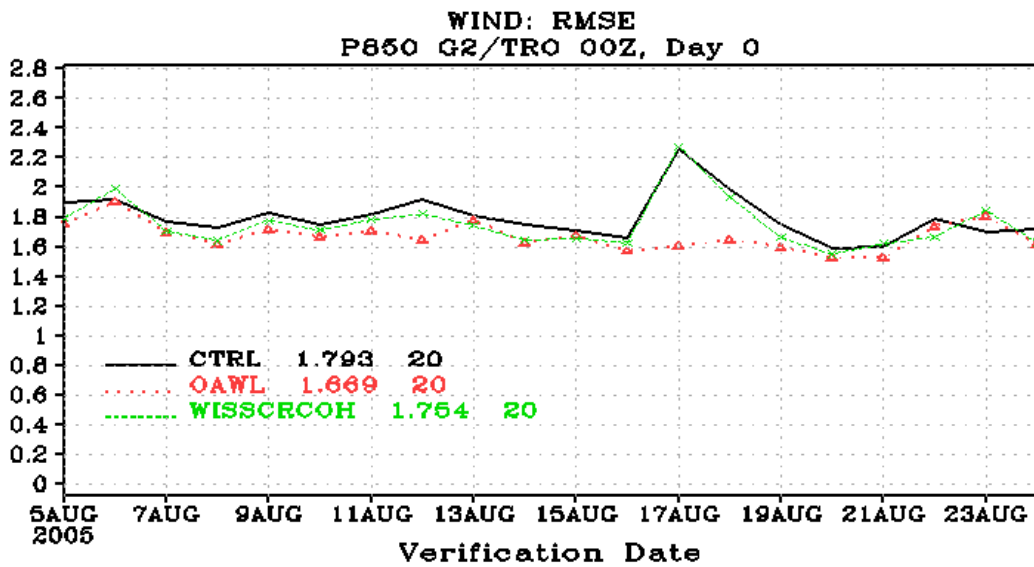
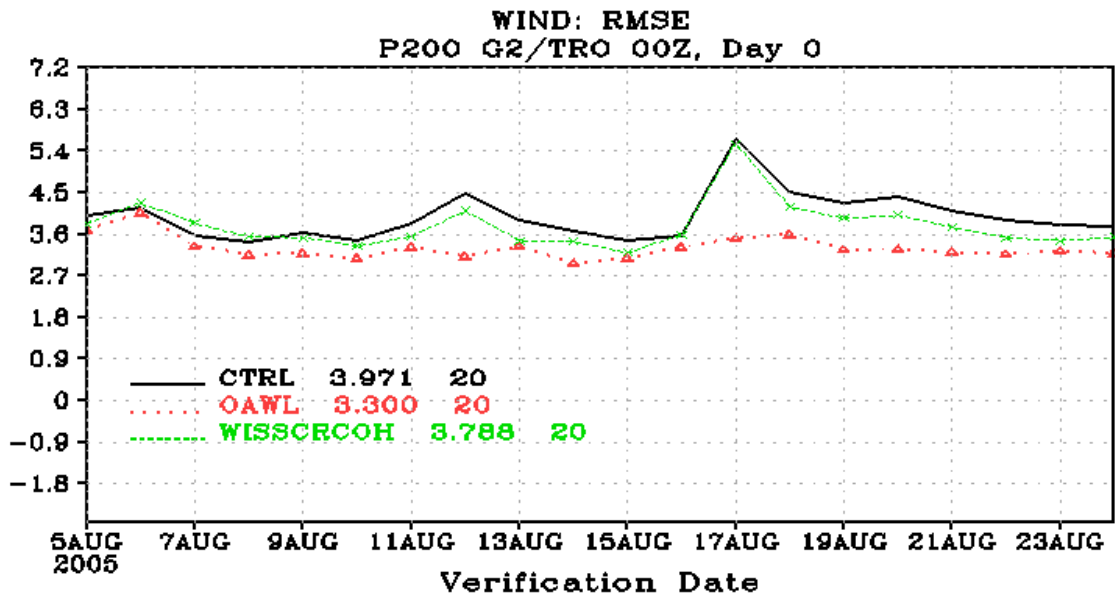


Fig. 29. Time series of the vector wind RMSE at 200 hPa and 850 hPa for analyses verifying daily from 7 July through 15 August 2005 in the Tropical regions. Analyses for each run were initialized at 0000 UTC and verified against the Nature Run. CTRL (black), OAWL (red) and WISSRCOH (green).

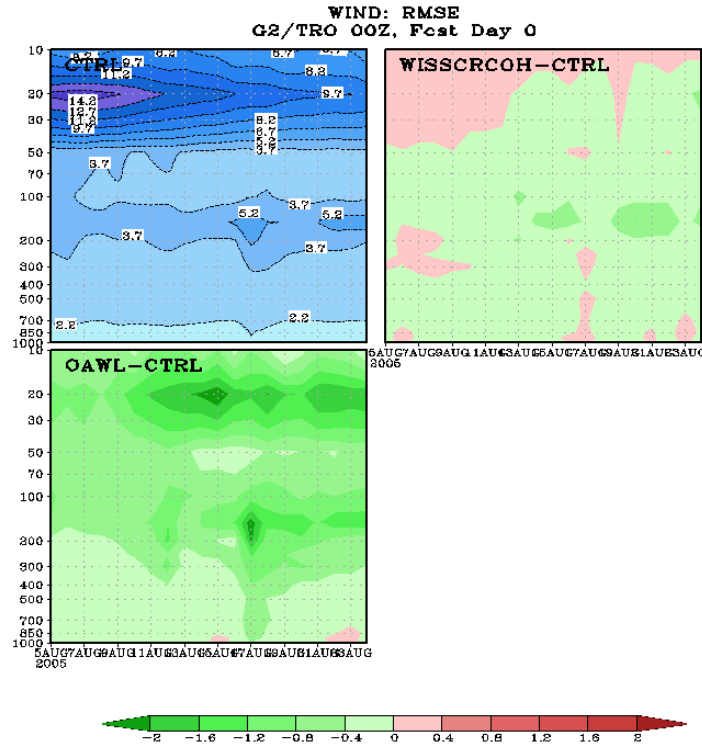


Fig. 30. The RMSE comparison of tropical vector wind analyses over the complete assimilation period. (a) Up-Left panel shows the time series of tropical wind RMSE from CTRL against Nature Run for each pressure level (from 1000 hPa to 10 hPa). (b) Another two panels show the difference between the RMSEs of lidar (OAWL and WISSRCOH) and CTRL runs, respectively. Red areas denote a negative lidar impact, green areas a positive impact.

In order to illustrate the wind lidar impact at different forecast ranges, vector wind RMSEs of the forecasts from these three runs versus the Nature Run at 200 and 850 hPa are shown for the tropics in Figure 31. The mean is calculated based on all cases at 0000 UTC each day. The values of vector wind RMSE are shown in the upper panel of each figure, and the differences from the CTRL are shown in the lower panel of each figure. Time 0 represents the analysis. At the 200 hPa pressure level, the benefit from the OAWL lidar wind data is readily apparent. Wind lidar observations from OAWL reduce the tropical wind RMSE by values ranging from 0.7 down to 0.14 ms^{-1} , depending on the range, while the corresponding reductions due to the coherent lidar observations from WISSCR_COH lie between. Similar results are found at the 850-hPa pressure levels, albeit with somewhat less pronounced error reductions.

Overall, the comparison of vector wind RMSE differences in the tropics shows that the experiments assimilating lidar wind data show greatly improved vector wind RMSE statistics compared to the CTRL. The largest lidar benefits appeared at upper levels for OAWL.

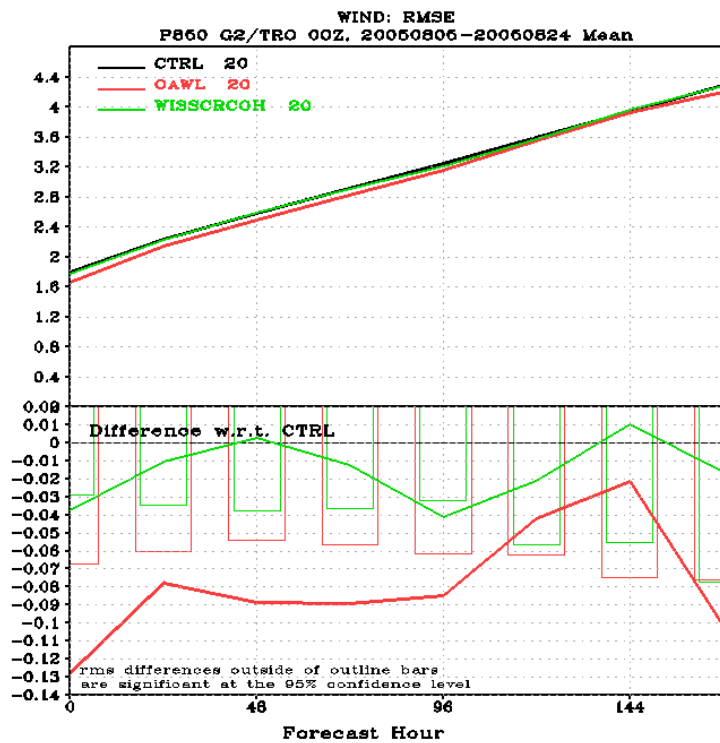
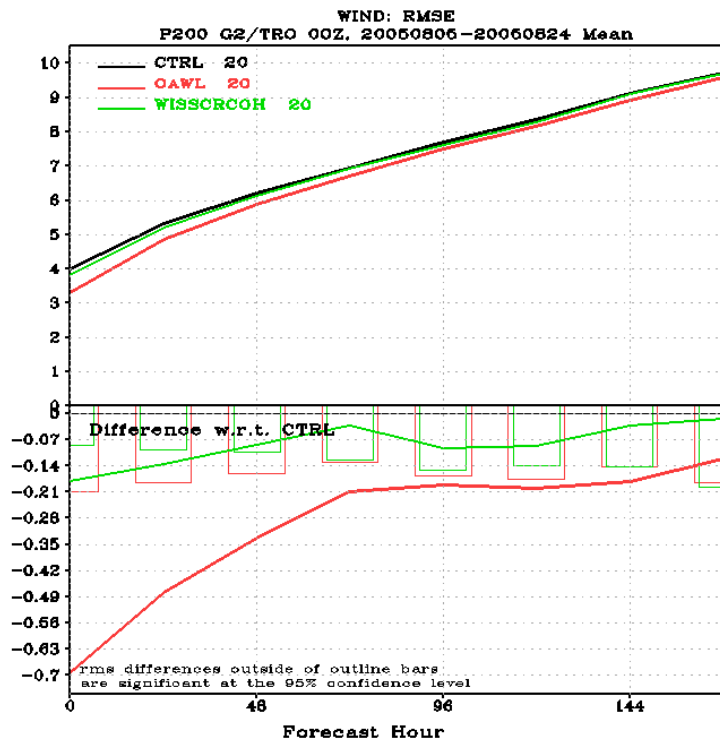


Fig. 31. The vector wind RMSE (m/s) by forecast time for CTRL (black), OAWL (red) and WISSCR_COH (green) forecasts verifying in the tropics at (left) 200 hPa and (right) 850 hPa. In the lower panel of each figure, the error bars represent the significance of the difference between the lidar (OAWL and WISSCRCOH) and CTRL runs at the 95% confidence level. Forecasts for each run were initialized at 0000 UTC and verified against the Nature Run.

7.2 GEOPOTENTIAL HEIGHT ANOMALY CORRELATION

In addition to the tropical winds, the Anomaly Correlation Coefficients (ACC) for the geopotential height fields at 500 hPa in the extratropics were calculated using the NCEP verification package. The anomaly correlation is defined as the correlation between the forecast and analyzed deviations (anomalies) from climatology (Holton, 1992). The following expression is used for computing the anomaly correlation of geopotential height at 500 hPa:

$$ACC = \frac{\sum \left\{ \left[(Z_F - Z_C) - \overline{(Z_F - Z_C)} \right] \left[(Z_V - Z_C) - \overline{(Z_V - Z_C)} \right] \right\}}{\sqrt{\sum \left[(Z_F - Z_C) - \overline{(Z_F - Z_C)} \right]^2 \sum \left[(Z_V - Z_C) - \overline{(Z_V - Z_C)} \right]^2}} \quad (3)$$

Here the suffix F denotes the forecast, suffix C denotes climatology, and suffix V indicates verification data (the Nature Run for these experiments). The over bar indicates the time mean and Z is the geopotential height at 500hPa. The summations in this equation are made over time.

Figure 32 displays time series of 500-hPa geopotential height anomaly correlation at day 7 in the Northern and Southern hemispheres. Values from all three experiments (CTRL, OAWL and WISSCR_COH) remain around 0.7 in the Northern Hemisphere and above 0.6 for most days in the Southern Hemisphere. Very large impact can be found some days, i.e., Aug 8 in NH and August 19 in SH. The means in the middle column of the legend for each panel are taken over all cases initialized at 0000 UTC during the the forecast period, and its sequence in NH is: CTRL (0.695) < WISSCR_COH (0.711) < OAWL (0.717). Similar results can be found in SH as well.

In Figure 33, we show anomaly correlation skill from the four OSSE 168-h forecasts at 500 hPa for the Northern and Southern hemispheres, respectively. The increase in AC skill in the two lidar runs over the CTRL is significant in the NH and SH, where the benefits of lidar are already noticeable at short-range forecasts (day 2) and increase with forecast time.

Figure 34 illustrates the relative impact of OAWL and WISSCR_COH for the day 7 forecast from August 19 in the SH. This figure shows that in general both lidars improve upon the control forecast, but the impact of OAWL is substantially larger in this case. It is extremely important to understand the nature of both large positive and large negative impacts whenever they occur. This will be the subject of future investigations, and will be used to optimize the assimilation of lidar data in future studies.

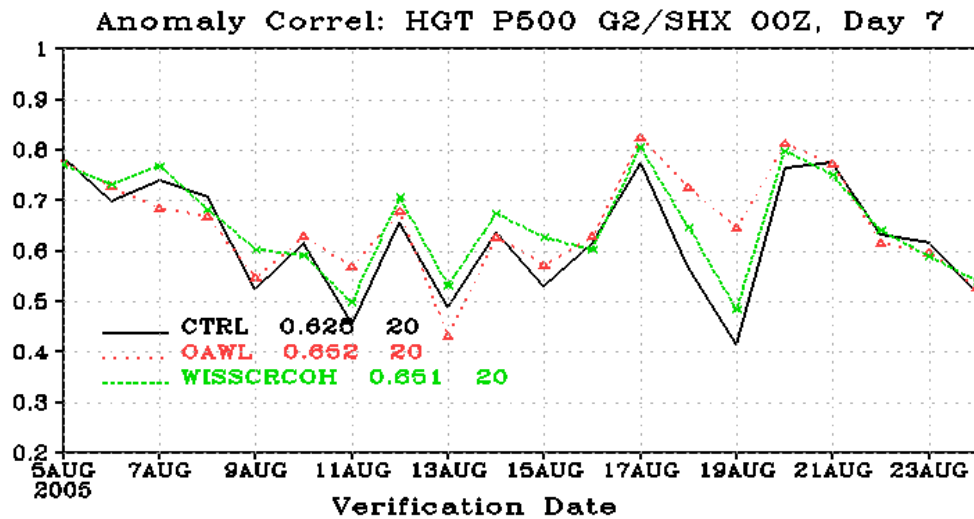
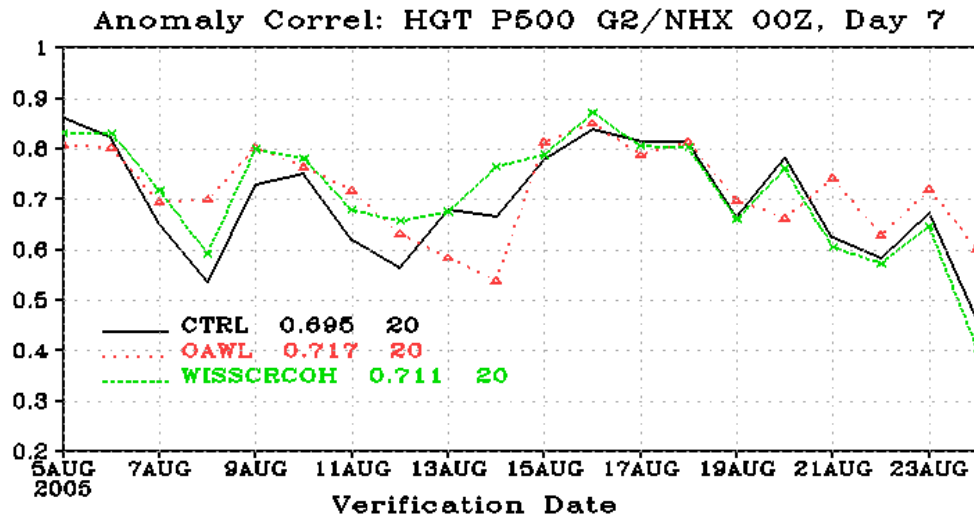


Fig. 32. Time series of the 500-hPa geopotential height anomaly correlation scores on Day 7 for CTRL (black), OAWL (red) and WISSCR_COH (green) forecasts verifying daily in the (Up) Northern and (Down) Southern Hemispheres. Forecasts for each run were initialized at 0000 UTC and verified against the Nature Run.

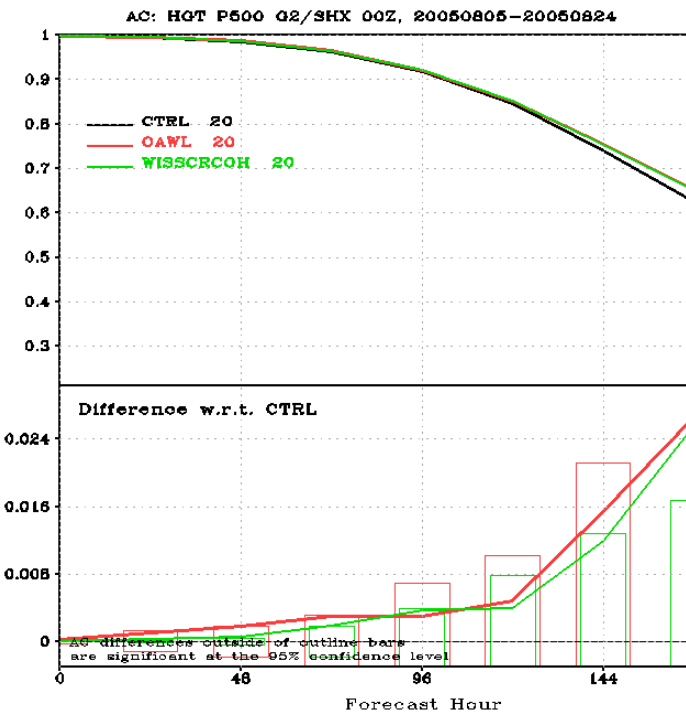
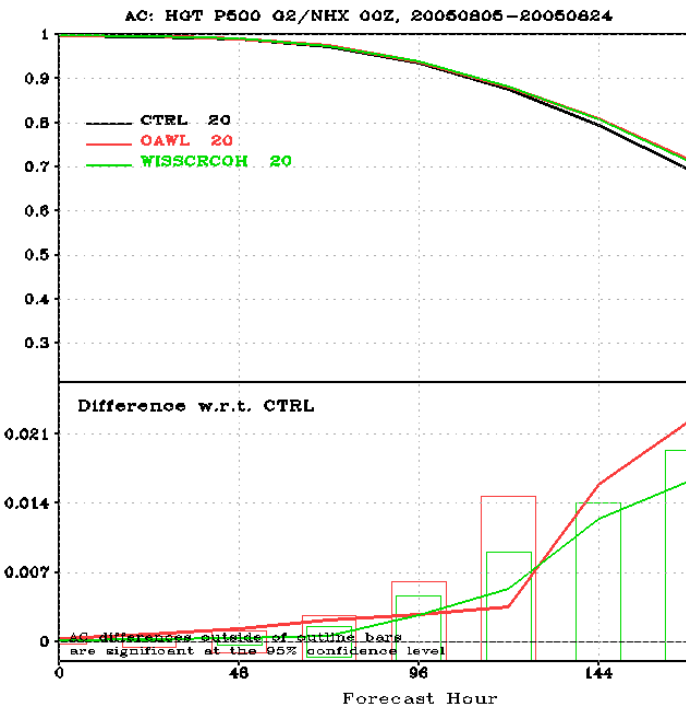


Fig. 33. The average 500-hPa geopotential height anomaly correlation scores by forecast time for CTRL (black), OAWL (red) and WISSCR_COH (green) forecasts verifying daily in the (left) Northern and (right) Southern Hemispheres. In the lower panel of each figure, the error bars represent the significance of the difference between the lidar (OAWL and WISSCR_COH) and CTRL runs at the 95% confidence level. Forecasts for each run were initialized at 0000 UTC and verified against the Nature Run.

Comparison of day 7 Forecast

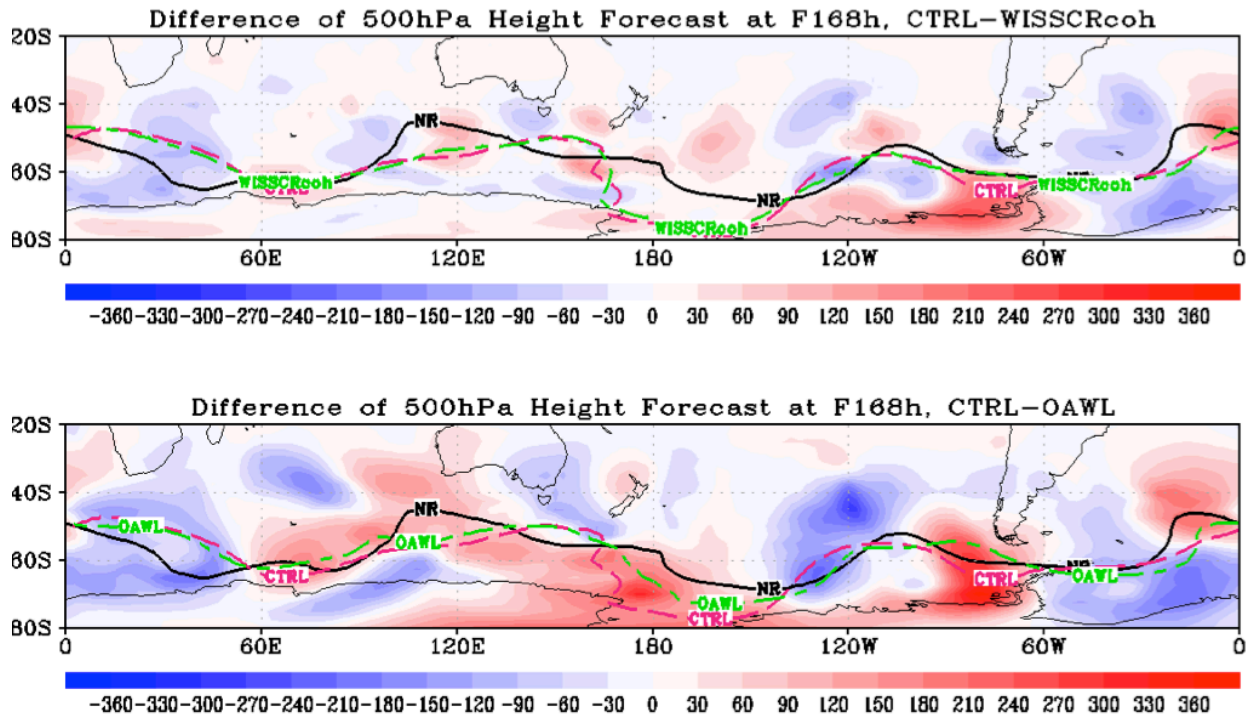


Fig. 34 Difference of 7-day 500 mb height forecasts from August 19 for Control minus WISSCR_COH (top) and Control – OAWL (bottom).

8. HWRF-GSI/WRF-ARW

The final set of experiments that we performed was aimed at evaluating the relative impact of OAWL and WISSCR_COH on hurricane track and intensity forecasting. For these experiments, SWA simulated 18 hours of enhanced OAWL and WISSCR_COH line of sight observations from the 1 km resolution WRF ARW nature run that had been embedded within the ECMWF T511 nature. Three assimilation cycles were performed, every 6 hours from August 4 06Z to August 4 18Z. The Control for these experiments assimilated all of the standard satellite and conventional data sets, using the HWRF/GSI system described in section 3c. This was followed by Control + WISSCR_COH and Control + OAWL assimilations, with three 114 hour forecasts generated after each analysis. (Output from the first Control + WISSCR_COH forecast was only available for the first 60 hours of the forecast at the time of this report.) All of these experiments used the JCSDA Control experiment for boundary conditions.

Figure 35 shows the sea level pressure rms error averaged over the forecast domain for the three Control, Control + WISSCR_COH, and Control + OAWL HWRF forecasts for the first 60 hours of model integration. At the initial time, all of the experiments show a similar error. The forecasts with WISSCR_COH data show a positive impact 6 hours into the forecast, and a negative impact thereafter. In contrast, the forecasts from initial conditions that included OAWL data display a distinct positive impact over the same time period.

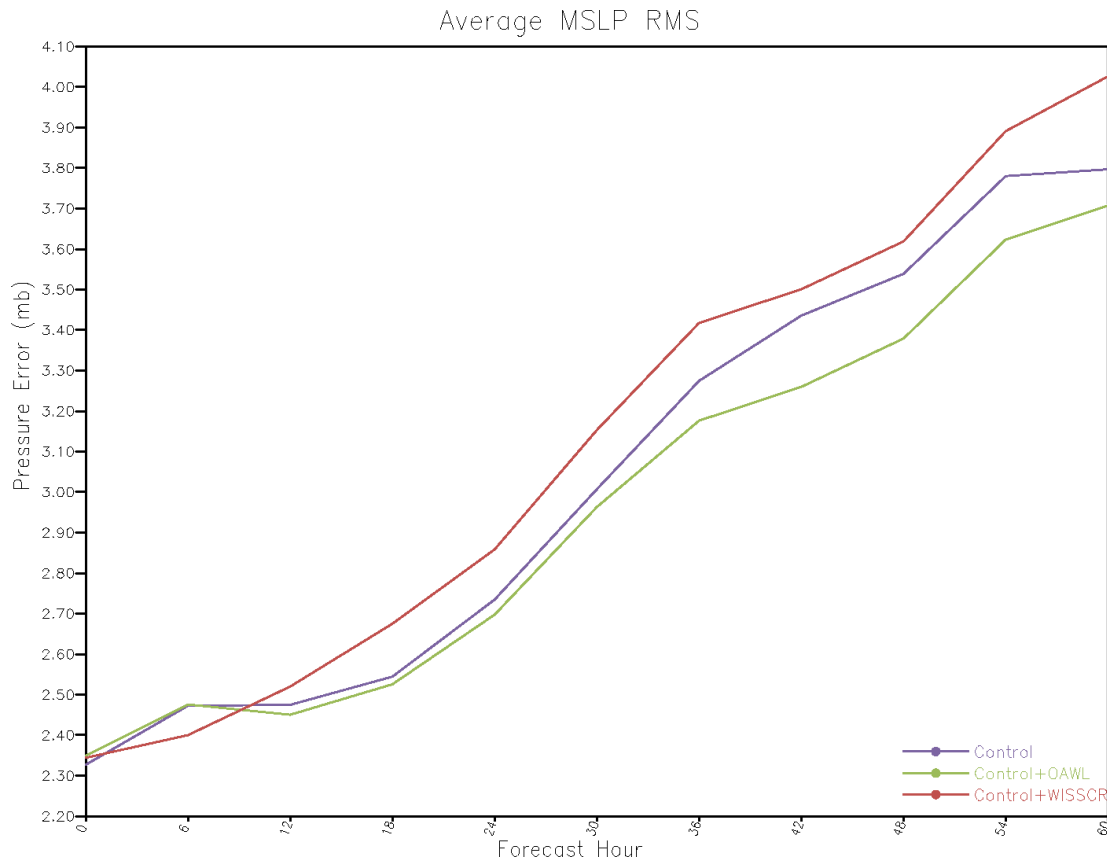


Fig. 35 Average sea level pressure rms errors for the 3 HWRF forecast experiments

The impact of OAWL and WISSCR_COH lidar observations on track forecasts is shown in figures 36-38. Two of the three forecast cases show a positive impact of lidar winds on the forecast track of the hurricane, with the OAWL data giving a substantially larger impact.

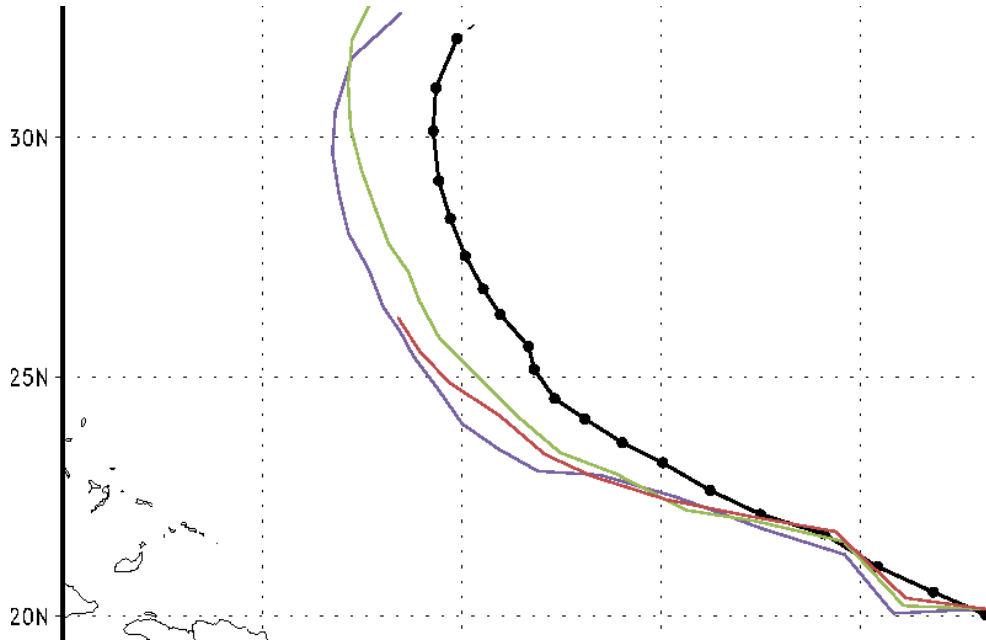


Figure 36 Track forecasts from August 4 06Z for Nature (black), Control (purple), Control+WISSCR_COH (red) and Control+OAWL (green).

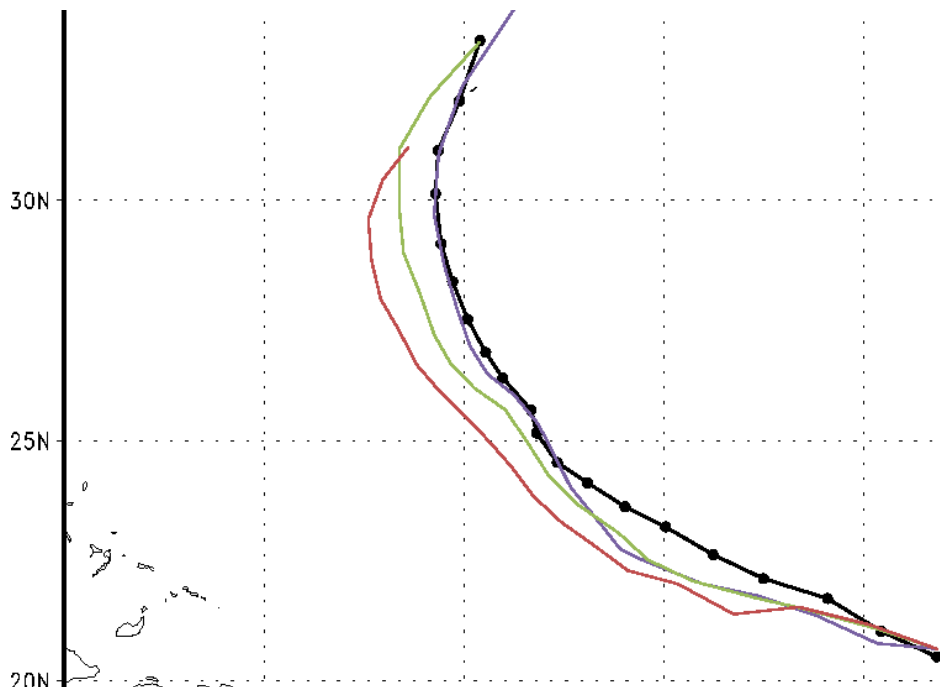


Figure 37 Same as Fig. 36 for forecasts from August 4 12Z.

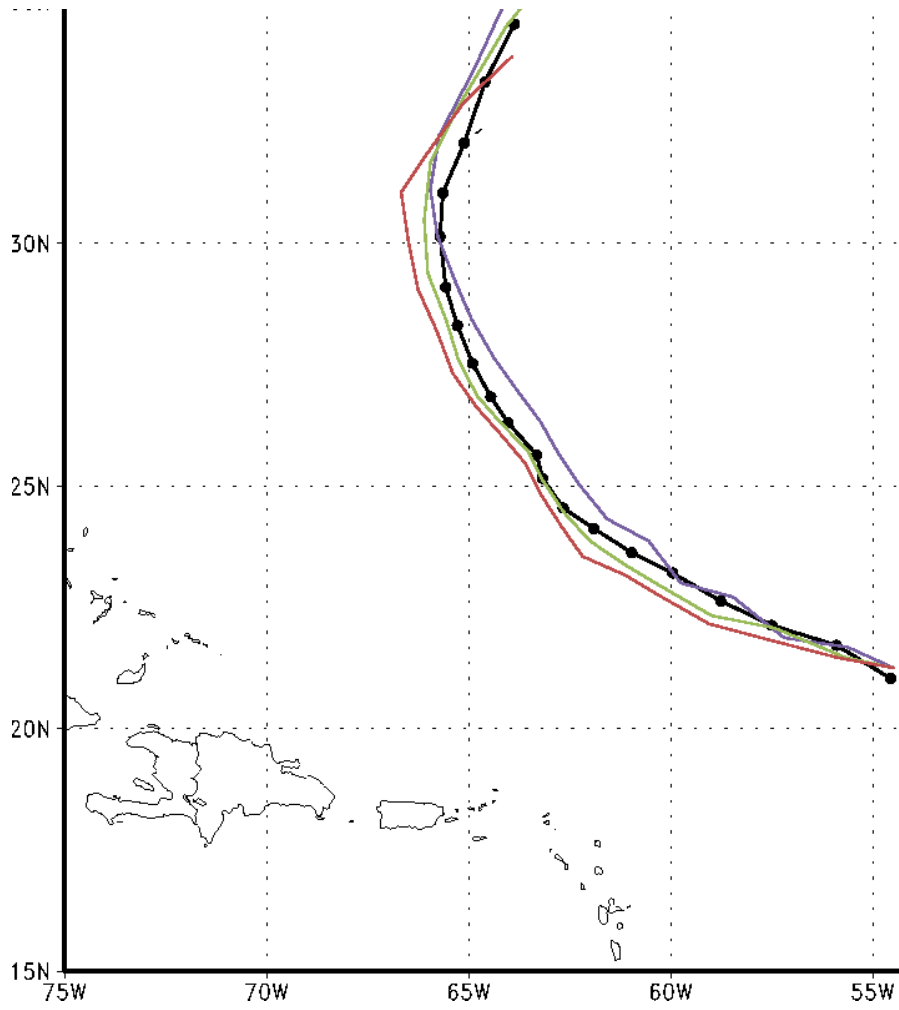


Fig. 38 Same as Fig. 36 for forecasts from August 4 18Z.

9. Summary and Recommendations

A study has been conducted to evaluate the potential impact of the Optical Autocovariance Wind Lidar (OAWL) on numerical weather prediction. The primary goal was to assess the advantages and disadvantages of using the OAWL technique in place of the current coherent DWL concept proposed for use in the WISSCR mission. To this end the OSSE team developed an agreed upon conceptual instrument model for OAWL, generated unique very realistic simulations of OAWL and WISSCR_COH data from three separate nature runs, performed an extensive lidar data product evaluation (a pre-OSSE), and performed OSSEs using two global OSSE systems and one state of the art regional OSSE system.

The primary conclusions from the pre-OSSEs comparisons are:

- The Energy Aperture Products (EAP) for the OAWL and companion DE detector are significantly higher than those for the WISSCR concepts. This disparity should be taken into consideration when making comparisons between the OAWL and WISSCR coherent instruments, but it does not offset other advantages of the OAWL technique.
- The vertical coverage of useful quality “aerosol winds” for the OAWL system is much greater than that for the WISSCR_coherent system. This is due not only to the larger EAP for OAWL, but that as a direct detection technique, the falloff in velocity measurement precision is not as precipitous as in the case of coherent detection. Another way to express this advantage is that OAWL can return an observation with 3m/s (or greater) precision when aerosols are more scarce than the design concentrations while the coherent system would not report an observation of less than 1.5m/s once the concentrations fell below a design threshold.
- The vertical coverage of the DE systems in the mid and upper troposphere are comparable for both mission scenarios. This fact explains why the team chose to focus on comparing just the aerosol subsystems in the OSSEs.
- The coherent system (WISSCR_coh) is the better PBL wind observing system while the OAWL provides more quality aerosol winds in the mid and upper troposphere. The coherent detection technique remains superior to the OAWL technique for producing high precision measurements in the presence of clouds and sufficient aerosols (primarily in the PBL).

The first global OSSE was conducted using the GEOS-5 DAS/fvGCM OSSE system, in part to determine if this system could be used to assess the relative value of the two different lidar systems. The results of this OSSE indicate little improvement when lidar wind profiles are assimilated, even in the cases where idealized data with unusually high quality and quantity are used. These results are in direct conflict with earlier OSSEs using validated OSSE systems. As discussed in section 6, this OSSE system had never undergone a rigorous validation, and there

are a number of inconsistencies between the data assimilation and nature run components. These inconsistencies appear to be responsible for the lack of meaningful impact and we concluded that this system could not be used to address the relative impact of differing lidar instruments. The only conclusion that could be drawn from this experiments was that the magnitude of impact is highly dependent upon the horizontal coverage of the data, ie. Increased coverage, such as that represented by a swath rather than a single line of data should result in a substantially larger impact. We recommend that lidar instrument developers explore the possibility of enhancing horizontal coverage for space-based Doppler wind lidars, and that further OSSEs with “state of the art” OSSE systems be conducted to quantify the gain in analysis and forecast accuracy that would result from different coverage scenarios

The next global OSSE was conducted with a current state of the art OSSE system that used the ECMWF T511 nature run and the NCEP GFS for data assimilation and forecasting. This OSSE demonstrated that both lidar systems improved tropical wind analyses and forecasts, with the largest impact occurring in the upper troposphere. The percentage beneficial impact of OAWL was found to be more than three times as large as that for WISSCR_COH in reducing errors in wind analyses at both upper (16.9% for OAWL vs. 4.6% for WISSCR) and lower levels (6.9% for OAWL vs. 2.1% for WISSCR_COH) of the troposphere. Substantially larger impact for OAWL is also true at nearly every forecast interval out to 7 days for tropical wind. Both lidars also demonstrated beneficial impact on 500 mb height forecasts for both the Northern and Southern Hemisphere Extratropics. The impact is largest in the Southern Hemisphere, where the percentage increase in forecast skill (as represented by the anomaly correlation) is nearly identical for both lidars (+4.1% for OAWL vs. +4.0% for WISSCR_COH). In the Northern Hemisphere Extratropics, the beneficial impact of OAWL (+3.1%) is larger than that for WISSCR_COH (+2.3%). This OSSE did show considerable case-to-case variability, with examples of negative as well as positive impact of OAWL relative to WISSCR_COH and of either lidar relative to the control. We recommend that case studies be conducted to document and understand the nature of both the large positive and large negative impacts that occurred. This would contribute to improved utilization of space-base lidar winds in the near future. It would also be desirable to increase the sample size for these experiments.

The final OSSE that we performed utilized a 1 km resolution WRF ARW nature run embedded within the ECMWF T511 nature, and NOAA’s Hurricane Prediction System, currently consisting of the HWRF forecast model coupled with the GSI analysis. The results of this OSSE indicate considerable potential for lidar wind data to improve hurricane forecasts, but substantially more work is required to (1) increase the sample size, (2) study and understand the nature of both the positive and negative impacts that occur, and (3) to optimize the assimilation of lidar winds in order to obtain consistent forecast improvements. In the limited hurricane forecast experiments that we have performed thus far, the OAWL data has proved more useful than WISSCR data. However, these experiments have only examined the effect of improving initial conditions. Both lidars could also provide data to improve the model physics and thus contribute to improved predictions through this effect as well.

The most general conclusion from this study is that the OAWL instrument operating at .355 micrometers would be capable of making significant improvements to atmospheric analyses and numerical forecasts. We recommend that further OSSEs be conducted to (1) increase sample

size, (2) diagnose the large impact cases that occur to improve the assimilation of Doppler wind lidar data, and (3) determine the optimal configuration for space-based lidar winds in terms of coverage and accuracy.

References

Atlas, R., E. Kalnay, and M. Halem, 1985a: The impact of satellite temperature sounding and wind data on numerical weather prediction. *Optical Engineering*, 24, 341-346.

Atlas, R., E. Kalnay, W.E. Baker, J. Susskind, D. Reuter, and M. Halem, 1985b: Simulation studies of the impact of future observing systems on weather prediction. *Proceedings, 7th AMS Conference on Numerical Weather Prediction*

Atlas, R., 1997: Atmospheric observations and experiments to assess their usefulness in data assimilation. *Journal of the Meteorological Society of Japan*, 75, 111-130.

Atlas, R., and G.D. Emmitt, 2008: Review of observing system simulation experiments to evaluate the potential impact of lidar winds on numerical weather prediction. *ILRC24*, Vol. 2 (ISBN 978-0-615-21489-4), 726-729.

Atlas, R., and L. P. Riishojgaard, 2008: Application of OSSEs to observing system design. *Proc. Of SPIE*, **7087**, doi: 10.1117/12.795344.

Atlas, R., 2012: Observing system simulation experiments to assess the impact of remotely sensed data on hurricane prediction. *Proceedings, SPIE Symposium on Optical Engineering and Applications*, August 12-16, 2012, San Diego, California. International Society for Optics and Photonics, SPIE 8515-26, 8 pp.

Atlas, R., G. D. Emmitt, and T. Pagano, 2013: Observing system simulation experiments to evaluate the impact of remotely sensed data on hurricane track and intensity prediction. *Proceedings, SPIE Symposium on Optical Engineering and Applications*, August 2013, San Diego, California. International Society for Optics and Photonics, SPIE 8 pp.

Bloom, S. C., L. L. Takacs, A. M. da Silva, D. Ledvina, 1996: Data assimilation using Incremental Analysis Updates. *Mon. Wea. Rev.*, **124**, 1256-1271.

Emmitt, G. D., J. Spinhirne, R. Menzies, D. Winker and D. Bowdle, 2001: Target Atmospheres for use in DWL Concept Studies. Submitted to the New Millennium Program by An Ad Hoc Committee.

Emmitt, G.D. and S.A. Wood, 1996. Simulating clouds within a space-based Doppler lidar wind sounder simulation model. Paper presented at the Cloud Impacts on DOD Operations and Systems 1995 Conference, Hanscom AFB/Phillips Laboratory, October, 1995.

Masutani, M., L. P. Riishojgaard, J. S. Woollen, Z. Ma, T. Zhu, D. Emmitt, S. A. Wood, S. Greco, H. Sun, F. Weng, D. Groff, M. Lueken and Y. Xie, 2012: Joint OSSEs at NOAA, Calibration Evaluation of DWL, JPSS, and DWSS. Jan 26, 2012

Nolan, D., R. Atlas, K. Bhatia and L. Bucci, 2013: Development and validation of a hurricane nature run using the joint OSSE nature run and the WRF model. *Journal of Advances in Modeling Earth Systems.*, 5, 382-405.

Rienecker, M. M., and Coauthors, 2008: The GEOS-5 data assimilation system – Documentation of versions 5.0.1, 5.1.0, and 5.2.0. *Technical Report Series on Global Modeling and Data Assimilation*, 27, 1-118.

Riishojgaard, L. P., Z. Ma, M. Masutani, J. S. Woollen, G. D. Emmitt, S. A. Wood, and S. Greco, 2012: Observation System Simulation Experiments for a Global Wind Observing Sounder, *Geophys. Res. Lett.*, 39, L17805, doi: 10.1029/2012GL051814.

Riishojgaard, L.P., Z. Ma, M. Masutani, J. Woollen, G.D. Emmitt, S.A. Wood, S. Greco, 2012: Wind Lidar OSSEs in the Joint Center for Satellite Data Assimilation. Working Group on Space-Based Lidar Winds. Coconut Grove, Florida, May 1 - May 2.

Talabac, S. J., and Coauthors, 2011: A sensor web simulator: Project status and the benefits to the atmospheric sciences. *15th Conference on Integrated Observing and Assimilation Systems for the Atmosphere, Oceans, and Land Surface*, 23-27 January, Seattle, WA.

Wilks, D. S., 1995: *Statistical Methods in the Atmospheric Sciences*. Academic Press, San Diego, 467 pp.

Wood, S., G.D. Emmitt, and S. Greco, 2001: The challenges of accessing the future impact of space-based Doppler wind lidars while using today's global and regional atmospheric models. AMS 5th Symp. Integrated Observing Systems, Albuquerque, NM, January.

Wood, S., G. Emmitt and S. Greco, 2000: DLSSM: A coherent and direct detection lidar simulation model for simulating space-based and aircraft-based lidar winds. Proceedings SPIE's 14th Annual Internat. Symp. Aerospace Defense Sensing, Simulation and Controls, Orlando, FL,

World Meteorological Organization, 2011: *Manual on Codes: International Codes*. WMO No. 306, Volume I.2, Part B.